STUDY OF SILVER DEPOSITION ON SILICON (100) BY IR SPECTROSCOPY AND PATINA FORMATION STUDY OF OXYGEN REDUCTION REACTION ON RUTHENIUM OR PLATINUM

Fan Yang, B.S.

Thesis Prepared for the Degree of

MASTER OF SCIENCE

UNIVERSITY OF NORTH TEXAS

August 2009

APPROVED:

Oliver M.R. Chyan, Major Professor
Guido F. Verbeck, Committee Member
Michael G. Richmond, Chair of the Department of Chemistry
Michael Monticino, Dean of the Robert B. Toulouse School of Graduate Studies

Yang, Fan. Study of Silver Deposition on Silicon (100) by IR Spectroscopy and Patina Formation Study of Oxygen Reduction Reaction on Ruthenium or Platinum. Master of Science (Chemistry), August 2009, 67 pages, 34 figures, 2 tables, references, 77 titles.

To investigate conditions of silver electroless deposition on silicon (100), optical microscope, atomic force microscope (AFM) and attenuated total reflection infrared spectroscopy (ATR-FTIR) spectroscopy were used. Twenty second dipping in 0.8mM $AgNO_3$/4.9% solution coats a silicon (100) wafer with a thin film of silver nanoparticles very well. According to AFM results, the diameter of silver particles is from 50 to 100nm. After deposition, arithmetic average of absolute values roughness (R_a) increased from ~0.7nm to ~1.2nm and the root mean square roughness (R_q) is from ~0.8nm to ~1.5nm. SCN^- ions were applied to detect the existence of silver on silicon surface by ATR-FTIR spectroscopy and IR spectra demonstrate SCN^- is a good adsorbent for silver metal.

Patina is the general name of copper basic salts which forms green-blue film on the surface of ancient bronze architectures. Patina formation has been found on the surface of platinum or ruthenium after several scans of cyclic voltammetry in 2mM $CuSO_4$/0.1M K_2SO_4, pH5 solution. Evidence implies that oxygen reduction reaction (ORR) triggers the patina formation. ORR is an important step of fuel cell process and only few sorts of noble metals like platinum can be worked as the catalyst of ORR. Mechanisms of patination involving ORR were investigated by cyclic voltammetry, optical microscope, AFM, rotating disk electrode and other experimental methods: the occurrence of ORR cause the increase of local pH on electrode, and Cu^{2+} ions prefer to form Cu_2O by reduction. Patina forms while Cu_2O is oxidizing back to Cu^{2+}.

ACKNOWLEDGEMENTS

On the brink of completing my degree, I would like to acknowledge my appreciation to those who have encouraged and supported me to complete this period of education.

I greatly appreciate the efforts of my mentor and research advisor, Dr. Oliver M. R. Chyan for his countless support, encouragement and guidance during the course of research that I could benefit in my entire life of both profession and individual. I also appreciate my committee member, Dr. Guido F. Verbeck for his help to sharp my keen to the research of Analytical Chemistry in all respects. I would also like to thank Dr. Theresa Golden and other professors for their amazing teachings and profound courses. The financial support from Welch Foundation and UNT Faculty Research Fund is deeply appreciated.

Thanks to two of my present group members, Kyle Yu for teching and help with fundamental operations of electrochemical analyzer and electrode polishing, as well as Karthik S. Pillai for his teaching and help with ATR-FTIR technique. Thanks to excellent work from my previous group members, Dr. Yibin Zhang, Oscar Ojeda and Shyam S. Venkartaraman on the research of patina formation. I also appreciate other group members, Daniel Taylor and Pofu Lin, who have made this research group a pleasure to work with.

I would like to thank my family, who has provided me with constant affection and encouragement. I would like to express my deepest appreciation to my wife, Dongyuan Zhao, for her unwavering support and love. I would like to thank my parents and parents-in-law for their long time support and confidence in my decision as well.

At last, I appreciate one of my best friends, Dizhi Wang who authorized the use of his picture of Statue of Liberty to assist me finishing this work.

TABLE OF CONTENTS

Page

LIST OF TABLES

Page

LIST OF FIGURES

Page

CHAPTER 1

INTRODUCTION

The purpose of this chapter is to introduce advanced analytical techniques and explain fundamental knowledge concerning interfacial and electrochemistry related studies. For better understanding, attenuated total reflectance with Fourier transform infrared (ATR-FTIR) spectroscopy, atomic force microscopy (AFM), cyclic voltammetry (CV), rotating disk electrode (RDE), and other surface and electrochemistry are briefly discussed in this chapter.

My research work concentrated on improving electrochemistry and surface science techniques. Thin films of silver, copper and their compounds are studied on silicon and noble metals' surface. Hopefully, the results of these experiments will not only clarify the mechanism of reactions, but also assist the industry of semiconductor and electronics. The aim of this introductory chapter will provide fundamental knowledge of experiment and research. Chapter 1 starts with preparing, cleaning, and modifying of silicon ATR crystals and surface modification techniques of silicon, basic knowledge of electrochemistry, and a brief introduction of AFM, CV and RDE. Chapter 2 is focused on electroless deposition of silver nano-particles on silicon and application of AFM and ATR-FTIR to measure the surface morphology and chemi-absorbance on silver surfaces. In chapter 3, the issue of oxygen reduction reaction with patina formation on platinum or ruthenium surface is discussed and CV and RDE techniques are used.

1.1 Silicon

Silicon is one of the elementary components of most integrated circuits (IC), optoelectronics, microelectronics, and microchips. Silicon is widely used in semiconductor industries due to its unique properties: it can remain a semiconductor at higher temperatures than

germanium and its native oxide can be easily grown in a furnace and form as better semiconductor/dielectric interface than any other materials [1, 2].

1.1.1 Structure of Silicon Crystal

Silicon (Si) and other group IV elements form face-centered diamond cubic crystal structures. Silicon atom forms four equal covalent bonds with other Si atoms in a tetrahedral shape [2]. Each Si atom is sp^3 hybridized in its diamond structure that has a fcc Bravais lattice [3]. Single crystal Si is a crystalline solid where the crystal lattice of the entire sample is continuous. Single crystal Si wafers are commercially available and widely applied in industry [4]. The (100) and (111) planes are the most popular Si single crystal wafers using for IC processing.

Figure 1.1 illustrates the orientation structure of both Si (100) and Si (111). The Miller index is used to name the set of integers and these integers are acquired from the reciprocal of the intercepts by the atomic plane to a three dimensional x, y and z axes. Figure 1.2 shows the lattice structure of Si (100) and Si (111) orientation planes. From both Figure 1.1 and Figure 1.2, it is clear that (100) plane has a square shape and (111) plane is in triangular shape. In this case, the fragments of (100) crystals have right angles and that of (111) fragments will have 60° triangles [5]. In the coming chapter 2, Si (100) ATR crystal was used to develop smooth hydride surfaces for silver (Ag) reduction on a Si surface.

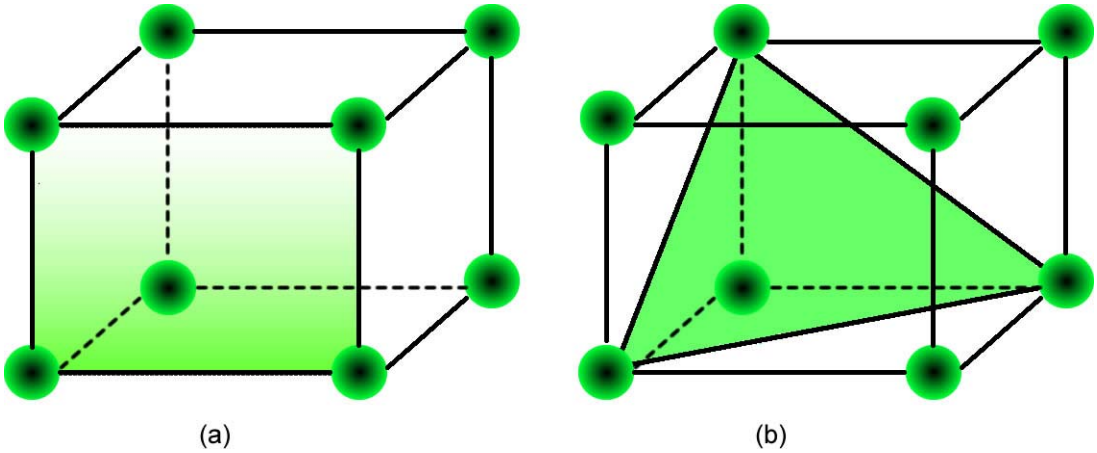

Figure 1.1 Miller indices structure for (a) Si (100) and (b) Si (111) planes.

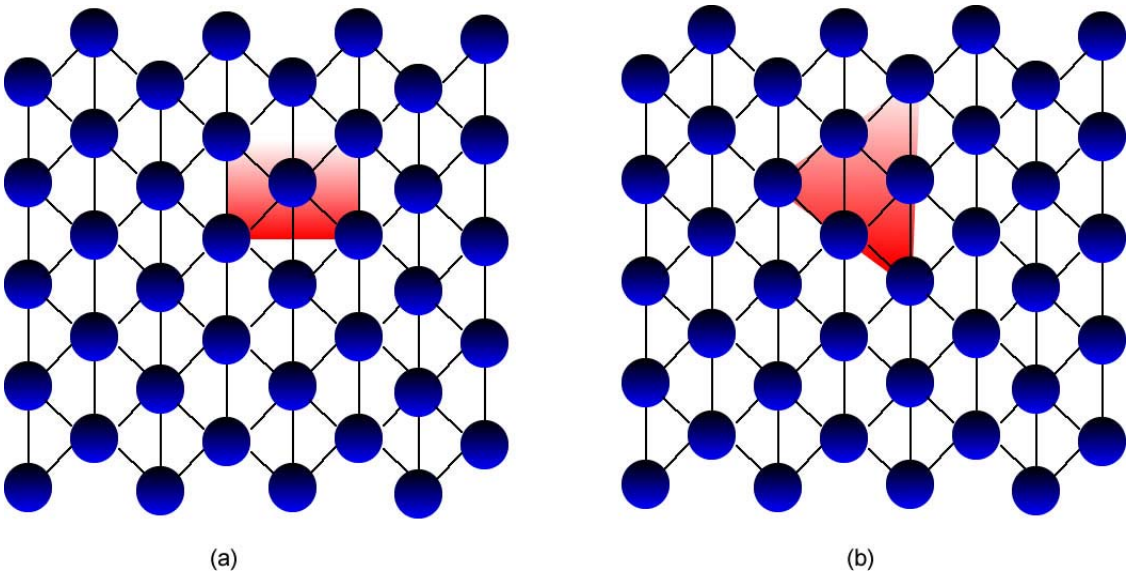

Figure 1.2 Lattice structure of (a) Si (100) and (b) Si (111) orientation planes.

1.1.2 Silicon ATR Crystal Preparation

Double polished silicon N-type phosphorus doped Si (100) (Wacker Co.) wafers with a resistivity of 0.6 – 1.0 Ohm·cm were used to prepare silicon attenuated total reflection (ATR) crystals. The silicon ATR crystals were cut from wafers with the dimension of 6cm × 1cm ×

0.7cm. Two ends of crystal were polished to a fineness of 1 micron by a rotating polishing pad from High Tech Allied Products. The ATR crystal was clamped by a sample holder at 45° to the plane of the rotating platen of polishing machine and the platen was rotated with the speed of 100 rpm along the bevel surface. A 30 micron grit size pad was used first to coarsely polish the bevel face for approximately 10 minutes, and continuous water flow flushed away any particles from the pad during polishing. Later, 15, 9, 3 and 1 micron pads were used to continue polishing the bevel face. When 3 and 1 micron grit pads were used, blue lube solution was used instead of water while polishing. All polishing pads and accessories were from Allied High Tech Products. (www.alliedhightechproducts.com)

After polishing, Si ATR crystals with both 45° bevel faces were subjected to wet etching cleaning using the RCA cleaning method to remove contaminants on the surface. The RCA cleaning was developed by Radio Corporation of America. It includes several chemical steps. Two major steps are named standard cleaning – I (SC1) and standard cleaning – II (SC2).

SC1 cleaning is required to remove organic contaminants from a Si surface. SC1 solution is a mixture of ultra pure water (UPW), ammonium hydroxide (NH_4OH) and hydrogen peroxide (H_2O_2) in a ratio of 5:1:1. Si ATR crystal was sequentially rinsed and sonicated with UPW and isopropyl alcohol (IPA) after polishing and SC1 solution for 10 minutes at a temperature of 80°C. Hydrogen peroxide works as a strong oxidizing agent to oxidize the top layer of silicon and forms surface oxide, while ammonium hydroxide etches away the oxide layer. This process of oxide formation and etching away will remove most of organic contaminants and particles from the surface.

SC2 cleaning is used to remove the metallic impurities from a silicon surface. SC2 solution is a mixture of UPW, H_2O_2 and HCl in the ratio of 5:1:1. ATR crystal is immersed in

this solution for 10 min at a temperature of 80°C. HCl dissolves all metal particles from surface, and then hydrogen peroxide oxidizes the silicon surface. During this process, alkali and metal contaminants are removed that were left from SC1 cleaning.

In diluted hydrofluoric acid etching method, hydrofluoric acid (HF) is applied to remove the oxide layer from the silicon surface [6, 7]. HF solution is dangerous and should be used with care [8, 9]. The concentration of HF typically for etching is 4.9%. It reacts with silicon dioxide which is given as

$$4HF + SiO_2 \rightarrow SiF_4 + 2H_2O \quad (1)$$

$$SiO_2 + 6HF \rightarrow 2H^+ + SiF_6^{2-} + 2H_2O \quad (2)$$

The SiF_4 is formed by the reaction of SiO_2 and HF. As a result, the Si-F bond polarizes the Si-Si bond in the second layer of the substrate. This process renders the silicon surface to be hydrogen terminated, making it extremely hydrophobic. This Si-H surface behaves as a source of electrons for reduction of Ag^+ ions. This is described with details in chapter 2.

The piranha solution is a mixture of concentrated sulfuric acid (H_2SO_4) and hydrogen peroxide (H_2O_2) used to remove organic contaminants from the surface. The solution is a strong oxidizer that assists in removing organics and it will also make the surface more hydrophilic. Many different mixture ratios like 4:1 or even 7:1are commonly used, but a typical mixture is 3:1 of concentrated sulfuric acid and hydrogen peroxide (30%). The following reaction equation explains the ions formed in the Piranha solution.

$$H_2SO_4 + H_2O_2 \rightarrow H_3O^+ + HSO_4^- + O \quad (3)$$

The atomic oxygen species formed in the solution allows the Piranha solution to dissolve the elemental carbon. The sulfate ions help in removing metals as soluble complexes. The substrate is exposed for about 10-15 minutes at a temperature of 100°C [10].

1.1.3 Electroless Metal Deposition on Silicon

Several techniques can be applied for depositing a thin metal film on the surface of substrates. These techniques include electron beam evaporation, electrochemical deposition, physical vapor deposition (PVD), chemical vapor deposition (CVD) and laser ablation. Electroless deposition is one of the techniques that are widely used in semiconductor industries. In chapter 2, I discuss the electroless deposition of silver (Ag) on silicon substrate for making Ag/Si material for chemical adsorption studies. Metal deposition on hydrogen terminated silicon surfaces has been studied widely in recent years [11, 12]. Metals that were reduced on hydrogen terminated silicon surface had to have more positive reduction potential (+0.34V vs. SHE) compared with hydrogen (0.00V vs. SHE) and be stable. Metal such as Cu, Ag, Au and Pt will be of this kind. Deposition of metal on a hydrogen terminated silicon surface without external applied potential is known as electroless deposition. This kind of methods is based on the electrochemical phenomenon that involves reduction of metal ions on silicon leading to deposition and oxidation of silicon [11]. The metal ion reduction could be expressed as:

$$M^{n+} + ne^{-} \rightarrow M \qquad (4)$$

During the electroless deposition process, the metal is deposited on the surface of a substrate through transferring electrons between a metal ion and a reducing agent in the solution. Hydrogen terminated solution is used as a reducing agent in electroless deposition of Ag on Si during this experiment.

1.2 Silver, Copper, Platinum and Ruthenium

Silver has been known since ancient times and has long been valued as a precious metal, used to make jewelry, high-value tableware, utensils and currency coins. Silver metal is used

today in electrical contacts and conductors, in mirrors and in catalysis of chemical reactions [12]. Its compounds are used in photographic film and dilute solutions of silver nitrate and other silver compounds are used as disinfectants. Among all metals, silver has the highest conductivity and the highest optical reflectivity. Silver also has the lowest contact resistance of any metal [13]. Silver is stable in pure air or water, but it will tarnish when exposed to air or water containing ozone or hydrogen sulfide to form a black layer of silver sulfide. The most common oxidation state of silver is +1; in addition, its +2 compounds and +3 compounds are well known as well [1].

Copper is a ductile metal with very high conductivity. Pure copper is soft and malleable, and a freshly exposed surface of copper has a pinkish or peachy color [1]. It is used as a thermal conductor, an electrical conductor, a building material and a constituent of various metal alloys [14]. Copper compounds are known in several oxidation states, where they often impart blue or green colors to natural minerals and have been used historically widely as pigments. Copper +2 ions are soluble in water, where they function at low concentration as bacteriostatic substances and fungicides. Copper is a metal that does not react with water, but the oxygen of the air will react slowly at room temperature to form a layer of brown-black or green-blue oxide on copper metal [15].

Platinum is a dense, malleable, ductile, precious and gray-white transition metal. It is resistant to corrosion and occurs in some nickel and copper ores along with some native deposits [16, 17]. Platinum is used in jewelry, laboratory equipment, electrical contacts and electrodes. The most common use of platinum is working as the catalyst in chemical reactions. It has been employed as catalysts since the early 1800s, when platinum powder was used to catalyze the ignition of hydrogen. Platinum also strongly catalyzes the decomposition of hydrogen peroxide

into water and oxygen gas [1, 18].

Ruthenium is found associated with platinum ores and used as a catalyst in some platinum alloys. Due to its ability to strengthen platinum or palladium, ruthenium is added in platinum and palladium alloys to make wear-resistant electrical contacts [19]. Owing to its lower cost and similar properties compared to rhodium, the use as plating material for electric contacts is one of the major applications of ruthenium [1]. The coatings are either put on by electroplating or sputtering. Ruthenium is also a catalyst with various applications. Hydrogen sulfide can be split by light by using an aqueous suspension of cadmium sulfide particles loaded with ruthenium dioxide. This may be useful in the removal of hydrogen sulfide from oil refineries and from other industrial processes. Certain ruthenium complexes absorb light via the visible spectrum and are being actively researched in various, potential, solar energy technologies. Ruthenium-based dyes have been used as the electron providers in dye-sensitized solar cells, a promising new low-cost solar cell system [19].

1.3 Background and Theory of ATR-FTIR Spectroscopy

1.3.1 Total Internal Reflection

A phenomenon of refraction could be explained as when a beam of light passes from a denser medium to a rarer medium, it will bend away from the normal direction to the rarer medium. If the light is totally reflected back into the denser medium, it refers to the phenomenon of total internal reflection.

1.3.2 Attenuated Total Reflection

Attenuated total reflection (ATR) is a modeling technique applied in conjunction with

infrared spectroscopy which enables samples to be checked directly in a solid or liquid state without future preparation [10, 20]. It is important to know and discuss the theory and background of ATR-FTIR spectroscopy since this technique has been widely used in my experiment. ATR applies a property of total internal reflection named the evanescent wave, the phenomenon which was recorded by Newton in the early 1700s. Extensive study has been done after the 1970s in this realm with the advent of molecular detected instrumentations like FTIR etc. Merits that make this technique unique refer to its simplicity in sampling and sensitivity of information derived from it.

In ATR-FTIR spectroscopy, the IR radiation gain propagates through the internal reflection element (IRE) and brings an evanescent electrical field that decays with Z axis. For internal reflection to happen, two types of media should be in contact with each other: a denser medium with high refractive index (such as Silicon, 3.42) and a rarer medium that is the thin film of sample on the surface of silicon. Figure 1.3 illustrates the schematic working process of ATR-FTIR. From the diagram of Figure 1.3, the angle of incidence of IR radiation should be greater than the critical angle θ_c, which is a function of the refractive index of both the sample and IRE [21, 22].

$$\theta_c = \sin^{-1}(n_2/n_1) \tag{5}$$

Where n_2 is refractive index of sample and n_1 is refractive index of ATR material. The number of refractions of IR radiation depends on the dimensions of ATR material. Basically, an ATR material has the size of 6cm×1cm×0.7 cm with the bevel surface polished to an angle of 45°. Typically, the number of reflections that can be achieved will be up to 100 times. The total number of reflections (N) of a given length (L) and width (W) of an ATR material is given by:

$$N = (L/W) \cot \theta_c \tag{6}$$

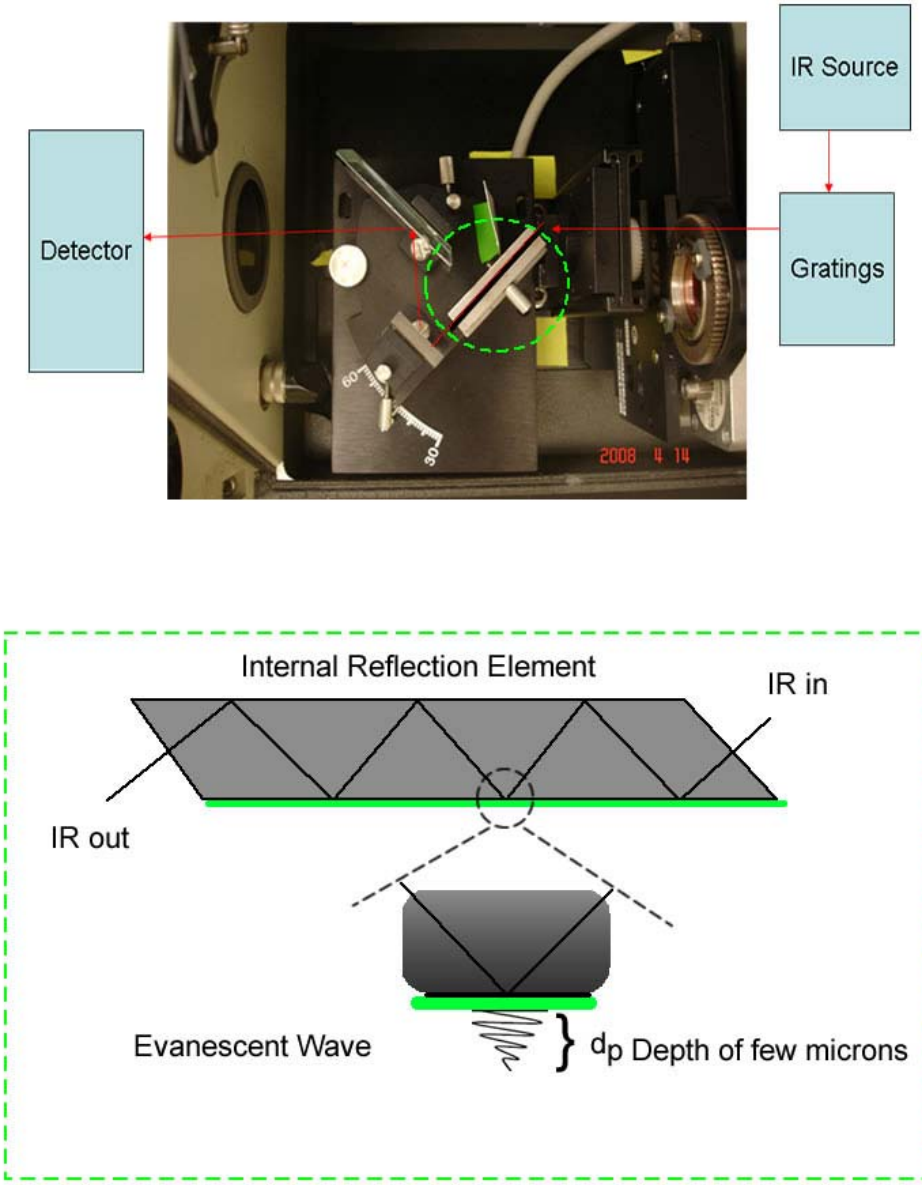

Figure 1.3 Schematic representation of ATR-FTIR spectroscopy.

The evanescent wave is an electrical field (E), which is produced normal to the reflecting surface. The exponential decay of the evanescent wave is in the order of microns and depends on the energy of IR radiation. If E_o is considered to be the amplitude of the incident energy, then E, the amplitude of the evanescent wave can be expressed as [23]

$$E = E_o \exp [-(2\pi/\lambda_1)(\sin^2\theta-(n_2/n_1))]^{1/2}Z \quad (7)$$

Where$\lambda_1=\lambda/n_1$ is the wavelength of radiation in silicon ATR, λ is the wavelength of radiation in air and Z is the distance from the surface. Harrick [21] deduced this equation by taking into account the energy absorption in the rarer medium as ,

$$E = E_o \exp [-\gamma Z] \quad (8)$$

Decay constant,

$$\gamma = 2\pi[\sin^2\theta-(n_2/n_1)^2]^{1/2}/\lambda_1 \quad (9)$$

The penetration depth of the evanescent wave is expressed as $d_p = 1/\gamma$. That is,

$$d_p =\lambda_1/2\pi(\sin^2\theta-(n_2/n_1)^2)^{1/2} \quad (10)$$

Where λ_1 is the wavelength of IR radiation, n_1 is the refractive index of the ATR element and n_2 is that of sample medium. A sample calculation of penetration depth is shown at wavenumber 400 cm^{-1} (25 μm) with angle of incidence 45°, d_p = 6.18μm.

Hence the penetration depth can be controlled by varying angle of incidence or by choosing an IRE element. Various IRE elements have different refractive index. A list of elements with their refractive indexes is provided in the following table.

Table 1.1 List of commonly used IRE elements.

IRE Element	Refractive Index
Aluminosilicate	1.547
AgBr	2.16
AgCl	1.98
Germanium	4
KRS 5 (Thallium bromide/Thallium Iodide)	2.35
Silicon	3.42

In ATR spectroscopy, the bevels of ATR element crystals were shaped in such a way that the angle of their surfaces was 45°. The main advantage of using this ATR crystal is that it

undergoes multiple reflections with IR radiation which enables amplification of weak signals as a result of which the sensitivity is increased. It can detect up to sub-monolayer of substance.

1.4 Atomic Force Microscopy

Atomic force microscopy (AFM), one of scanning probe microscopes (SPM), was developed by Binnig, Quate and Gerber in 1986. The AFM is one of the prime tools for imaging, measuring and manipulating matters at nanoscales. Unlike scanning tunneling microscopy (STM), AFM does not need a conducting sample to record the contours of repulsion force developed by the overlapping of the electron cloud at the tip with those surface atoms [24-27]. Piezoelectric elements that facilitate tiny but accurate and precise movements on (electronic) command enable the very precise scanning.

The AFM consists of a cantilever in micron with a sharp needle-like tip at its end that is used to scan the sample surface. The cantilever is typically made of silicon or silicon nitride with a tip radius of curvature on the order of nanometers. It works as a spring to keep the tip against the surface when moving back and forth. When the tip is moved close to a sample surface, forces between the tip and the sample resulted in a deflection of the cantilever according to Hooke's law. Forces of 10^{-13} to 10^{-1} N are measured with AFM. Depending on the situation, forces that are measured in AFM include mechanical contact forces, Van der Waals forces, capillary forces, chemical bonding, electrostatic forces, magnetic forces, and so on. As well as force, additional quantities may simultaneously be measured through the use of specialized types of probe. Basically, a laser beam is located on the top of the tip and reflected to a photodiode sensor to measure the tiny movement of the tip. A feed-back regulator responds to the changes of the path by activating a piezoelectric control, which adjusts the height of sample to balance the force

between tip and surface. Topographic images of the sample are produced by translating the movement to the surface profile. This is enough to create fine resolution in atomic scales since the resolution can be reached to 1 or 2 angstroms when AFM examined a hard surface [28].

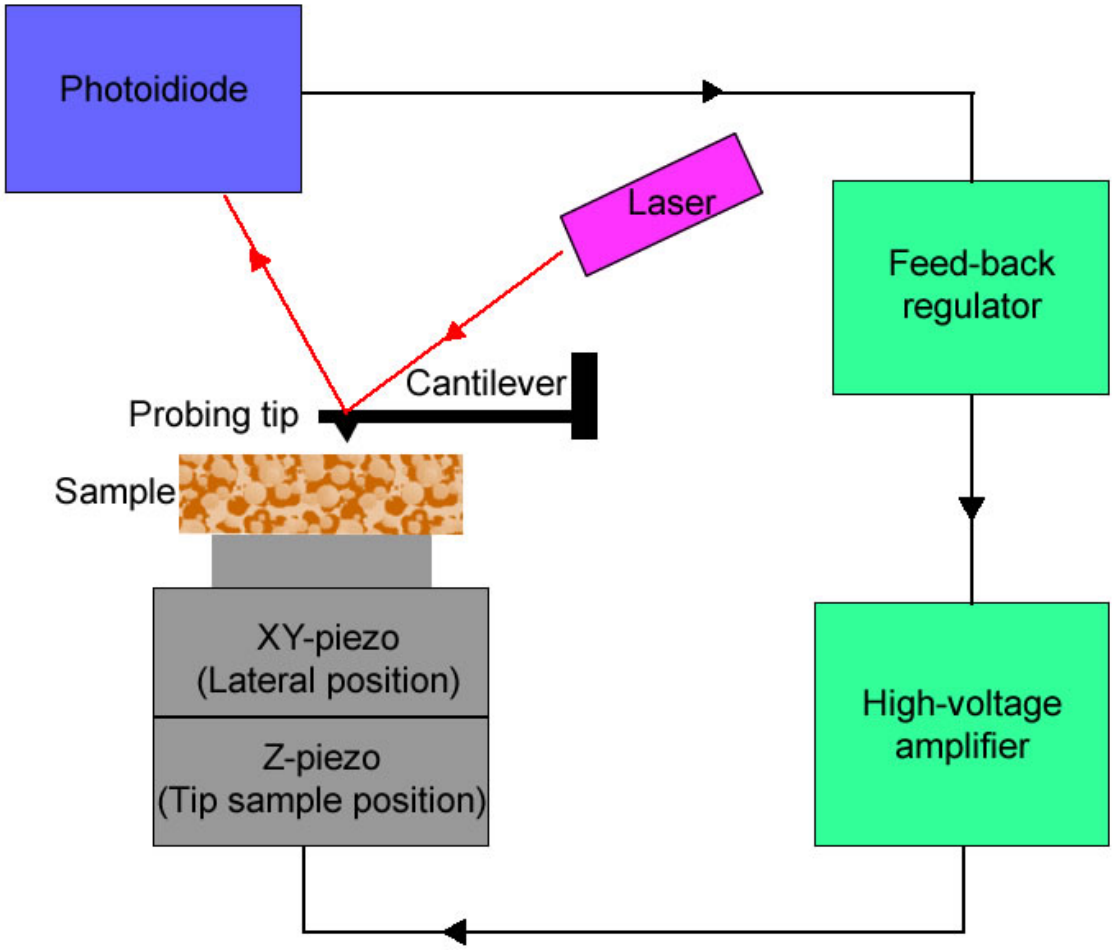

Figure 1.4 AFM working schematics.

In general, AFM modes are divided into contact (also called static) modes and a non-contact (or variety of dynamic) modes where the cantilever is vibrated. From the beginning, AFM was designed as a contact mode. However, it is hard to obtain a good image for a soft surface or a surface under liquid. Non-contact mode AFM, invented by Martin et al. [29], can solve those problems. In non-contact mode, the AFM tip should vibrate close to the surface of the sample with low energy due to the weakness of van der Waals forces. However, moving the

tip closer to the surface will increase the opportunities of sticking the tip in the water layer that covers the surface of all samples in the air, which can sharply degrade the quality of images. To improve the application of non-contact AFM, Digital Instruments (Veeco Inc.) has developed a new technique named Tapping Mode AFM (TM-AFM). In TM-AFM, larger vibration amplitude is given to the cantilever; therefore, the cantilever has sufficient energy to overcome the surface tension of the adsorbed water layer while vibrating through the sample. Conservative estimate predict the applied force to be in the 0.1 to 1 nano-Newton range, which is significantly lower than the force applied by the contact mode.

Nanoscope III Scanning Probe Microscope Multi-Mode® system (Veeco Inc.) is used to provide us surface information in Chapter 2 and Chapter 3. This system includes AFM, STM (scanning tunneling microscopy) and EC-AFM (electrochemical atomic force microscopy), and only AFM with J-type scanner (scan range from 2.5μm to 150) is applied in experiments. The set of an AFM consists of the optical head and the base. The stepper-motor, the alignment screws and the scanner are installed within the base, and the sample is mounted on the top of the scanner. The optical head contains a viewing window at the top, a laser diode, a set of mirrors, and a four-quadrant positional photo detector. The cantilever holder is firmed on top of the alignment screws, with the tip positioned over the sample. In order to align the laser beam to the top of the tip, an assistance of an optical microscope or a digital camera is needed.

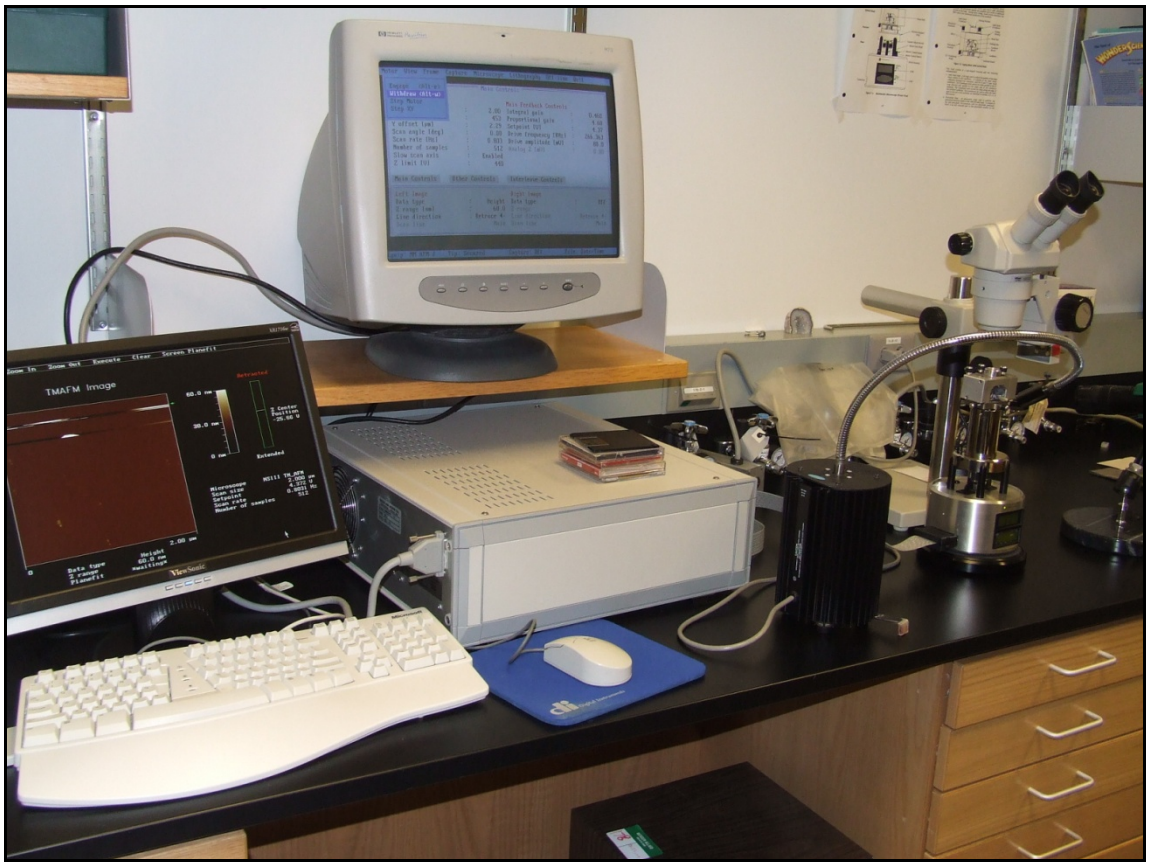

Figure 1.5 Nanoscope III SPM multimode systems.

1.5 Electrochemistry Techniques

1.5.1 Fundamentals of Electrochemistry

Electrochemistry is a branch of chemistry that studies chemical reactions which take place in a solution at the interface of an electron conductor such as a metal or a semiconductor and an ionic conductor (the electrolyte), and which involve electron transfer between the electrode and the electrolyte or species in solution. Electrochemistry was born in the late eighteenth century when scientists became interested in the production of electricity by animals such as the electric eel. From that time, electrochemistry has developed significantly and been applied in many areas in our life, such as plating metal, analysis, organic synthesis and energy storage [30].

If a chemical reaction is driven by an external applied voltage, as in electrolysis, or if a voltage is created by a chemical reaction as in a battery, it is an electrochemical reaction. Chemical reactions where electrons are transferred between molecules are called oxidation/reduction (redox) reactions.

In this research, cyclic voltammetry (CV) and rotating disk electrode (RDE) were used.

1.5.2 Three Electrode System

Electrochemistry experiments, especially voltammery experiments, investigate the half cell reactivity of an analyte solution. Most experiments control the potential of an electrode in contact with the solution while measuring the resulting current.

To conduct such an experiment requires at least two electrodes. The working electrode should apply the desired potential in a controlled way and facilitate the transfer of electrons to and from the analyte solution. A second electrode acts as the other half of the cell, which should keep a known potential with respect to the potential of the working electrode. In addition, it should balance the electrons added or removed by the working electrode. This one is called the reference electrode. Usually, the reference electrode is selected to have electrochemically active materials, with a composition that is independent by current, and connected in the low impedance circuit of a potentiostat. During the viable experiments, it has some disadvantages. One of them is that it is difficult for an electrode to maintain a constant potential while passing current to counter redox events at the working electrode [31].

To work out this problem, the role of supplying electrons and referencing potential has been divided between two separate electrodes. The reference electrode is a half cell with a known reduction potential. Its only role is to act as reference in measuring and controlling the

working electrode's potential and at no point does it pass any current. The counter (auxiliary) electrode passes all the current needed to balance the current observed at the working electrode. To achieve this current, the counter will often reach to extreme potentials at the edges of the solvent window, where it oxidizes or reduces the solution. These electrodes, the working, reference and counter make up the three electrode system [32].

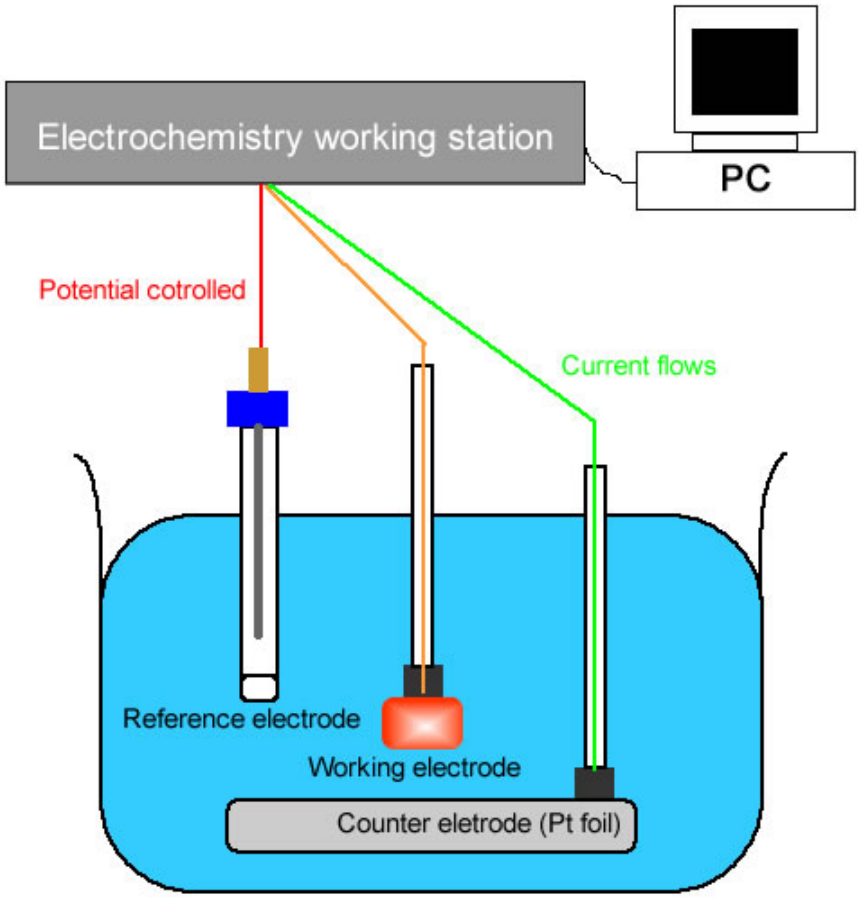

Figure 1.6 Schematic of three electrode system.

1.5.3 Cyclic Voltammetry

Cyclic voltammetry (CV) is a type of potentio-dynamic electrochemical measurement. In a CV experiment, the working electrode potential is ramped linearly versus time like linear sweep

voltammetry. Cyclic voltammetry takes the experiment a step farther than linear sweep voltammetry which ends when it reaches a set potential. When cyclic voltammetry reaches a set potential, the working electrode's potential ramp is inverted. This inversion can happen multiple times during a single experiment. The current at the working electrode is plotted versus the applied voltage to give the cyclic voltammogram trace. Cyclic voltammetry is generally used to study the electrochemical properties of an analyte in solution [33].

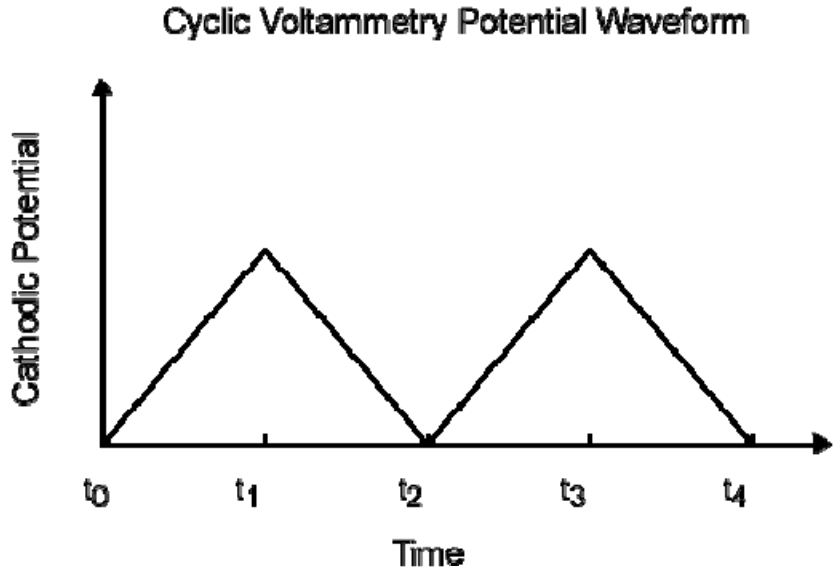

Figure 1.7 Cyclic voltammetry potential waveform.

In CV, the electrode potential ramps linearly versus time in CV. This ramping is known as the experiment's scan rate and the potential is measured between the reference electrode and the working electrode and the current is measured between the working electrode and the counter electrode [34]. This data is then plotted as current vs. potential. As the waveform shows, the forward scan produces a current peak for any chemical solution that can be reduced through the range of the potential scanned. The current will increase as the potential reaches the reduction potential of the solution, but then falls off as the concentration of the analyte solution is depleted

close to the electrode surface. If the redox couple is reversible, it will reach the potential that will re-oxidize the product formed in the first reduction reaction and produce a current of reverse polarity from the forward scan. This oxidation peak will usually have a similar shape to the reduction peak. As a result, information about the redox potential and electrochemical reaction rates of the compounds is obtained.

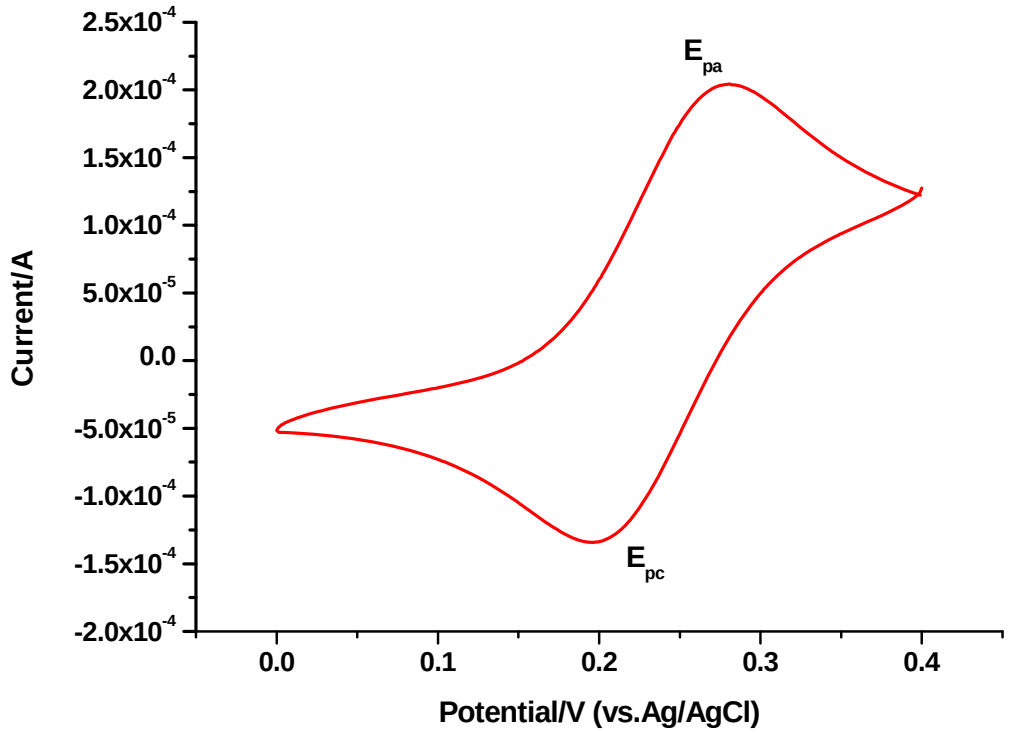

Figure 1.8 Cyclic voltammetry of 5mM potassium ferrocyanide and 0.1M potassium chloride.

1.5.4 Hydrodynamic Techniques

Hydrodynamic technique is a one of electroanalytical methods where the solution flows relative to a working electrode. When the working electrode is under the forced convection, the concentration of analytes remains constant [31].

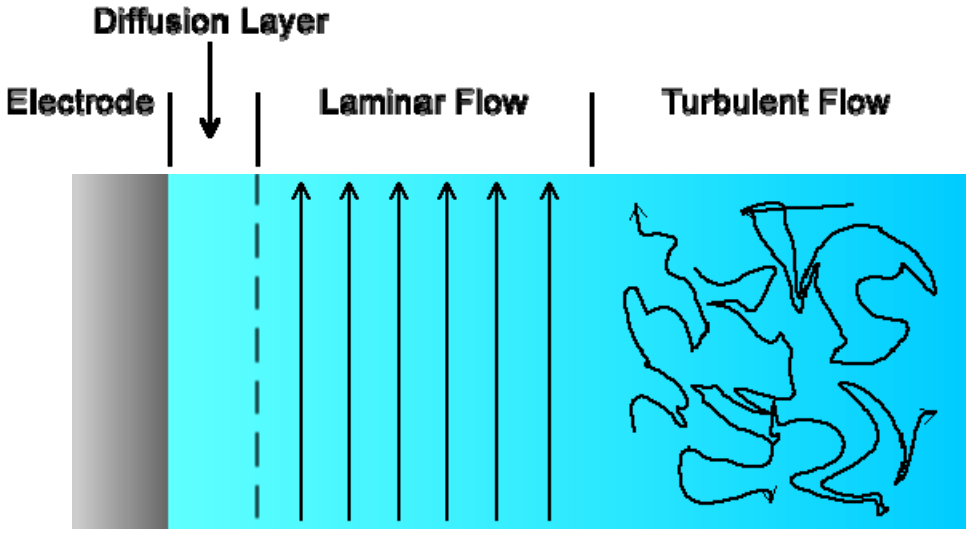

Figure 1.9 The electrode in solutions under hydrodynamic.

Showing in Figure 1.9, adjacent to the surface of the electrode is the Nernst diffusion layer. Under hydrodynamic conditions, the Nernst diffusion layer remains stagnant because of the frictional force between the solution and the electrode surface. Next to the Nernst diffusion layer is the laminar flow region in which the flow of the solution is parallel to the electrode surface. Any analyte outside the laminar flow region is named the turbulent flow region since not any specific direction of flow is at this area. The diffusion layer keeps thin and steadfast under hydrodynamic conditions because convection maintains the concentration of analytes throughout the laminar flow and turbulent flow regions. The solution is intentionally remains still to allow diffusion controlled mass transfer. When a solution is made to flow, through stirring (convection), it is important to the technique to obtain the controlled flow or mass transfer in order to achieve predictable results. These methods are types of electrochemical studies which apply potentiostats to investigate reaction mechanisms related to redox chemistry among other chemical phenomenon [31].

Hydrodynamics assist in the detection of analyte components as the increase in total flux leads to larger Faradaic currents. A magnetic stir bar could be used to mechanically agitate the solution. More often, a mechanical rotator equipped with rotating disk electrode (RDE) may be applied for more precise control over forced convection.

1.5.5 Rotating Disk Electrode

A rotating disk electrode (RDE) system is a hydrodynamic working electrode applied in a three electrode system [31]. The electrode rotates during experiments inducing a flow of analyte to the electrode. This method is used in electrochemical studies when investigating reaction mechanisms related to redox chemistry.

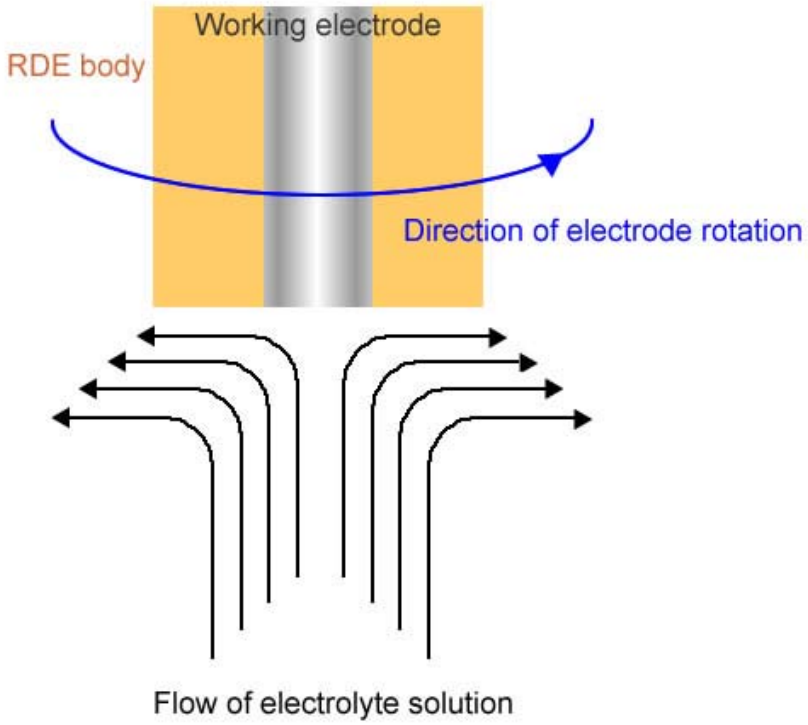

Figure 1.10 Solution movements by RDE rotating.

The electrode includes a conductive disk embedded in an inert non-conductive polymer or resin that can be attached to an electric motor that has fine control of the electrode's rotation rate. The disk, as the working electrode, is generally made of a noble metal or glassy carbon (GC); however, any conductive material can be used based on specific needs [35].

1.6 Chapter References

[1]. "The periodic table." webelements.com: http://www.webelements.com/. Retrieved on Feburary, **2008**.

[2]. "Silicon." Wikipedia: http://en.wikipedia.org/wiki/Silicon. Retrieved on March, **2009**.

[3]. Cotton, F.A.; Murillo, C.; *Advanced Inorganic Chemistry*, John Wiley & Sons; New York, **1999**.

[4]. Runyan, W.R.; Bean K.E; *Semiconductor Integrated Circuit Processing Technology*; Addison-Wesley Publishing Company: Reading, **1990**.

[5]. Hong, X; *Introduction to Semiconductor Manufacturing Technology,* Prentice-Hall Inc., Upper Saddle River, New Jersey, **2001.**

[6]. Burrows, V.A.; Chabal, Y.J.; Higashi, G.S.; Raghavachari, K. and Christman, S.B. *Applied Physics. Letter.* **1988**, 53, 998.

[7]. Chabal, Y.J.; Higashi, G.S.; Raghavachari, K. and Christman S.B. *Journal of Vacuum Science and Technology*, **1989**, A7, 2104.

[8]. Bertolini, J.C. *Journal of Emergency Medicine*, Vol. 10 pp 163 - 168, **1992**

[9]. Kirkpatrick, J. *Burns,* vol. 21, No. 7 pp 483 - 493, **1995**

[10]. "Piranha solution." Wikipedia: http://en.wikipedia.org/wiki/Piranha_solution. Retrieved on March, **2009**.

[11]. Lee, I.; Bae, S.; Song, M.; Lee, I.; Paek, S.; and Lee, C. *Bull. Korean Chem. Soc.* **2004**, 25, 2.

[12]. "Silver." Wikipedia: http://en.wikipedia.org/wiki/Silver. Retrieved on March, **2009**.

[13]. Edwards, H.W. and Petersen, R.P. *Phys. Rev.* 50 (9) 871, **1936**

[14]. "Copper." Wikipedia: http://en.wikipedia.org/wiki/Copper. Retrieved on March, **2009**.

[15]. Barnaby J. F. "Regulators Stamp Copper as a Germ Killer". http://www.nytimes.com/2008/03/26/business/26microbes.html?_r=1&scp=2&sq=copper&st=nyt&oref=slogin. *New York Times*. March 26, **2008**.

[16]. "Platinum." Wikipedia: http://en.wikipedia.org/wiki/Platinum. Retrieved on March, **2009**.

[17]. Woods, I. *The Elements: Platinum*. Benchmark Books. **2004**

[18]. Petrucci, R. H. *General Chemistry: Principles & Modern Applications* (9th edition). Prentice Hall. pp. 606. **2007**.

[19]. "Ruthenium." Wikipedia: http://en.wikipedia.org/wiki/Ruthenium. Retrieved on March, **2009**.

[20]. Ye, S.; Ichihara, T. and Uosaki, K. *Journal of the Electrochemical Society*, **2001,**148**,** 6, C421-C426.

[21]. Harrick, N.J., *Internal Reflection Spectroscopy*, Interscience Publishers, NY, **1967**.

[22]. FT-IR Spectroscopy—Attenuated Total Reflection (ATR). *Perkin Elmer Life and Analytical Sciences*, **2005**.

[23]. Mirabella, F.M.; Harrick, N.J. *Internal Reflection Spectroscopy; Review and Supplement*, Harrick Scientific Corporation, N.Y. **1985**.

[24]. Wickramashinghe, H. K. *Sci. Am.*, **1989**, 98.

[25]. Pool, R. *Science*, **1990**, 247, 634.

[26]. Binning, G.; Quate, C. F.; Gerber, C., Phys. *Rev. Lett.*, **1986**, 56, p930

[27]. Frommer, J.; Meywer, E. *J. Phys.*: Condens. Matter, 3, S1-S9 **1991**.

[28]. "Atomic Force microscope." Wikipedia: http://en.wikipedia.org/wiki/Atomic_force_microscope. Retrieved on March, **2009**.

[29]. Martin, Y.; Wichramasinghe, H. K. *Appl. Phys. Lett*. **1987**, 50, 1455

[30]. Kalvoda, R. and Parsons R., *Electrochemistry in Research and Development*, New York: Plenum press, **1985**.

[31]. Bard, A.J.; Faulkner, L.R. *Electrochemical Methods: Fundamentals and Applications***.** New York: John Wiley & Sons, 2nd Edition, **2000**

[32]. "Voltammetry." Wikipedia: http://en.wikipedia.org/wiki/Voltammetry#Three_electrode_system. Retrieved on March, **2009**.

[33]. "Cyclic voltammetry." Wikipedia: http://en.wikipedia.org/wiki/Cyclic_voltammetry. Retrieved on March, **2009**.

[34]. Vukmirovic, M. B.; Dimitrov, N.; Sieradzki, K., *J. Electrochem. Soc*, **2003**. 150 (1): p. B10-B15.

[35]. "Rotating disk electrode." Wikipedia: http://en.wikipedia.org/wiki/Rotating_disk_electrode. Retrieved on March, **2009**.

CHAPTER 2

STUDY OF SILVER DEPOSITION ON SILICON (100) BY FTIR-ATR SPECTROSCOPY

2.1 Introduction

In integrated circuit fabrication or semiconducting industries metal plating is always the popular research topic: especially when gold (Au), silver (Ag) or copper (Cu) particles deposit on silicon (Si) or another semiconductor wafer either chemically, physically or a combination of both methods. Plating describes a surface coating process that a metal is deposited on a conductive or semi-conductive surface. There are several plating methods and many applications [1]. Electroless plating, also known as chemical plating, is a non-galvanic type of plating method that involves several simultaneous reactions that happen without using external electrical power [2].

Silver is a good material for electroless plating. The resistivity and reliability for the sub 0.1 μm interconnect technology is the major factor limiting the development of metal plating. Silver is attractive for its lower resistivity, 1.59 μΩ·cm, and higher electro-migration resistance than Al, Cu [1-3]. Although different methods are applied in manufacturing thin metal films, electroless deposition is one of most excellent methods in ultra-large-scale integration interconnects due to its high aspects ratio and other features [2].

In this chapter, $AgNO_3$ and HF solutions were using to deposit nanoscale thin film Ag on Si (100) surface. From Nikon microscope images and AFM results, the thickness of Ag thin film is estimated to be about 50nm to 200nm. ATR-FTIR was using to measure the IR peak that indicates the existence of silver. However, the wave number of Ag-Si stretching bond is about 1,000 cm^{-1} that cannot be observed since there are many random H-Si peaks in this area. In this chapter, KSCN was selected as an adsorbent to label Ag particles. SCN^- is a good chemical to

bind with Ag and chemisorbs on Ag surfaces [4].

2.2 Experimental

2.2.1 Preparation of Silicon (Si) ATR Crystal

Double polished silicon N-type phosphorus doped Si (100) (Wacker Co.) wafers with a resistivity of 0.6 – 1.0 Ohm·cm were cut into pieces with dimensions of 6cm × 1cm × 0.7cm and polished at both ends with an angle of 45° using a multiprep polishing machine from Allied High Tech company. These polished Si pieces are applied as attenuated total reflection (ATR) crystals that are designed to undergo multiple internal reflections with infrared (IR) light. ATR crystals were also used as substrates for silver electroless deposition.

2.2.2 Cleaning of Silicon ATR Crystal

During the cleaning process; all lab wares used here were made of polyfluoroalkoxy material since hydrofluoric acids were used to treat the surface of silicon ATR crystal. These lab wares were cleaned many times in boiling solutions of 10% HNO_3 before they were employed in cleaning of silicon crystals.

After cutting and polishing, silicon ATR crystals would contain organic, inorganic and metallic contaminants on the surface. In order to remove these contaminants, the silicon crystals had to be cleaned by the following steps:

Ultra pure water (UPW) with resistance > 18.2 MΩ/cm was supplied via a Millipore Milli-Q® Elix5® ultra pure water purification system (Millipore Corp., Bedford, MA, www.millipore.com) for rinsing purposes as well as for any dilution of chemicals. The silicon crystal was initially rinsed and sonicated in UPW followed by rinsing with isopropyl alcohol

(IPA) and dichloromethane. High purity electronic grade HF, H_2O_2, NH_4OH and HCl (the chemicals were from Air Liquide, Dallas Chemical Center, www.airliquide.com) were used in cleaning of silicon crystals.

All silicon ATR crystals used were cleaned in hot solutions (70-80° C) of SC1 (Standard Cleaning I; 1:1:5; H_2O_2: NH_4OH: H_2O) and SC2 (Standard Cleaning I; 1:1:5; H_2O_2: HCl: H_2O) for 10 minutes. The crystals after cleaning from SC1 and SC2 were rinsed with UPW and purging with N_2 gas to remove solution resides.

After cleaning, silicon ATR crystals were immersed in 4.9% HF solution for 5 minutes. HF etching of cleaned silicon substrates removes oxide and terminates the surface with hydride. The hydride terminated silicon substrate was used for silver deposition by electroless plating technique. The IR spectra were taken after each experimental step.

After the IR measurements of hydride silicon crystal were taken, the bevel plane of the ATR crystal was covered with a hydrophobic Teflon tape before immersing it into the silver containing solution. The bevel surface should be protected by covering tapes from silver deposition so that IR light can pass through into the crystal and obtain correct reflections. Then the silicon hydride substrate was immersed in 50 ml of 4.9% HF solution containing silver ions of concentration 0.8 mM for a time period of 20 sec at room temperature. Ag^+ ions were reduced to metallic silver nanoparticles at the silicon surface. The silicon substrate was rinsed well with UPW after it was removed from the copper solution. The electroless plated silver film on silicon surface was observed through Nikon Eclipse ME600 optical microscope (Nikon, Japan) and AFM technique (Nanoscope III, Multimode scanning probe microscope, Veeco Inc.) to study the surface morphology. Then the IR spectrum of the Ag/Si was taken as a reference for chemi-adsorption. The ATR crystal was dipped in 5mM KSCN and 0.1M $KClO_4$ for 2 minutes,

rinsed with UPW and dried with pure N_2 gas. IR spectra were measured after each successive step using the same parameters. Figure 2.1 below illustrates a brief scheme for Si treatment, Ag electroless deposition and SCN^- adsorption.

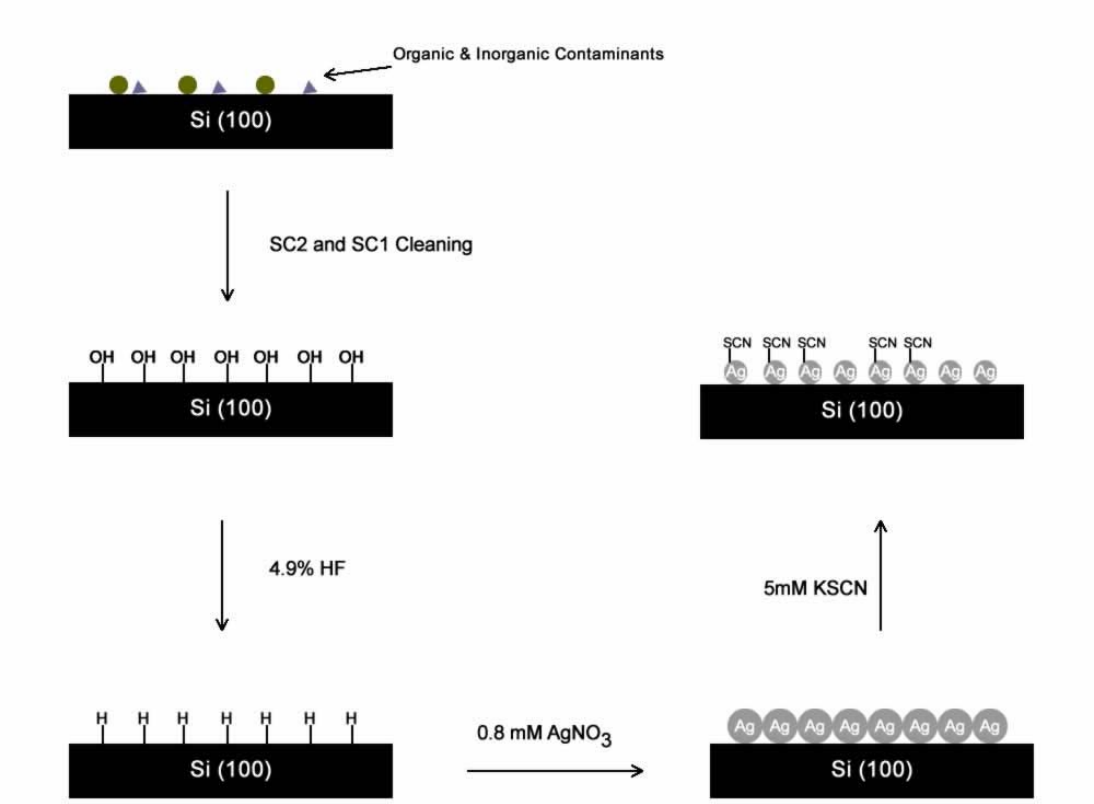

Figure 2.1 Scheme of Si treatment, Ag electroless deposition and SCN^- adsorbed process.

2.3 Results and Discussion

2.3.1 Microscopic and FTIR Results of Hydrogen Terminated Silicon Surface

After SC1 treatment, silicon ATR crystal was terminated with hydrogen coating using 4.9% HF solution. Since SC1 cleaning would cause the surface oxide for about 30 Å, after dipping in HF solution, surface will be etched away in the process of hydrogen termination. The hydrogen terminated silicon surface was microscopically smooth as can be seen from images from Nikon microscope and AFM images. A silicon wafer exposed to HF reacts with the surface

silicon oxide, SiO_2 as per the following reactions [5, 6]:

$$SiO_2\ (s) + 6\ HF\ (aq) \rightarrow H_2SiF_6\ (aq) + 2H_2O \quad (1)$$

$$H_2SiF_6\ (aq) \rightarrow SiF_4\ (g) + 2\ HF \quad (2)$$

2.3.2 Optimize Experimental Parameters of Electroless Silver Deposition

Metal deposition, especially gold, silver and copper, on silicon by electroless technique is more advantageous than other techniques in terms of uniformity, super-filling, simplicity and cost. The application of electroless deposition is vital in semiconductor industries. A series of experiments was done for the electroless Ag deposition in order to obtain smooth, fully covered and nano-ranged Ag particles on the Si surface. For the optimization of Ag deposition, a number of small Si (100) chips (1cm×1cm) were used.

The parameters that were under optimization include (1) concentration of Ag^+ ions, (2) concentration of HF solution, (3) time of deposition, and (4) pretreatment of silicon substrate. Table 2.1 lists series of experimental conditions to obtain a good silver deposition result. In the event of optimizing these parameters, it was observed through optical microscope that the Si crystal which undergone Ag deposition for 20s using 4.9% HF containing 0.8mM $AgNO_3$ (blue highlighted in the Table 2.1) had smooth and fully covered Ag particles on the surface as can be seen from microscope images in Figure 2.2. The major concern for this optimization of Ag deposition parameters is to achieve good "IR throughput". The IR throughput will be diminished totally if the deposited Ag thin film is too thick on the surface of the Si ATR crystal.

Table 2.1 Series of experiments conducted to produce uniform Ag nanoparticles on Si (100).

Cleaning Method	Hydrogen Terminated Solution	Cu Solution	Time of Deposition
SC1	4.9% HF	1mM $AgNO_3$/4.9% HF	30s
SC2	4.9% HF	1mM $AgNO_3$/4.9% HF	30s
Annealing 850°C 30 min	4.9% HF	1mM $AgNO_3$/4.9% HF	30s
SC2, SC1	4.9% HF	1mM $AgNO_3$/4.9% HF	30s
SC2, SC1	0.49% HF	1mM $AgNO_3$/4.9% HF	30s
SC2, SC1	0.049% HF	1mM $AgNO_3$/4.9% HF	30s
SC2, SC1	4.9% HF	2mM $AgNO_3$/4.9% HF	30s
SC2, SC1	4.9% HF	1.6mM $AgNO_3$/4.9% HF	30s
SC2, SC1	4.9% HF	1.2mM $AgNO_3$/4.9% HF	30s
SC2, SC1	4.9% HF	0.8mM $AgNO_3$/4.9% HF	30s
SC2, SC1	4.9% HF	0.6mM $AgNO_3$/4.9% HF	30s
SC2, SC1	4.9% HF	0.4mM $AgNO_3$/4.9% HF	30s
SC2, SC1	4.9% HF	0.8mM $AgNO_3$/4.9% HF	60s
SC2, SC1	4.9% HF	0.8mM $AgNO_3$/4.9% HF	40s
SC2, SC1	4.9% HF	0.8mM $AgNO_3$/4.9% HF	20s
SC2, SC1	4.9% HF	0.8mM $AgNO_3$/4.9% HF	10s

Before experiments, In the event of optimizing these parameters, it was observed through Nikon optical microscope that the Si crystal being treated with SC1 solution, that plated Ag deposition for 20s using 4.9% HF containing 0.8mM Ag^+ (highlighted in the table), had smooth and fully covered Ag particles on the surface as can be seen from microscope images. The major concern for this optimization of Ag electroless deposition parameters is towards the goal of

achieving good “IR throughput”. The IR throughput will be diminished totally if the deposited Ag film is too thick on the Si ATR crystal.

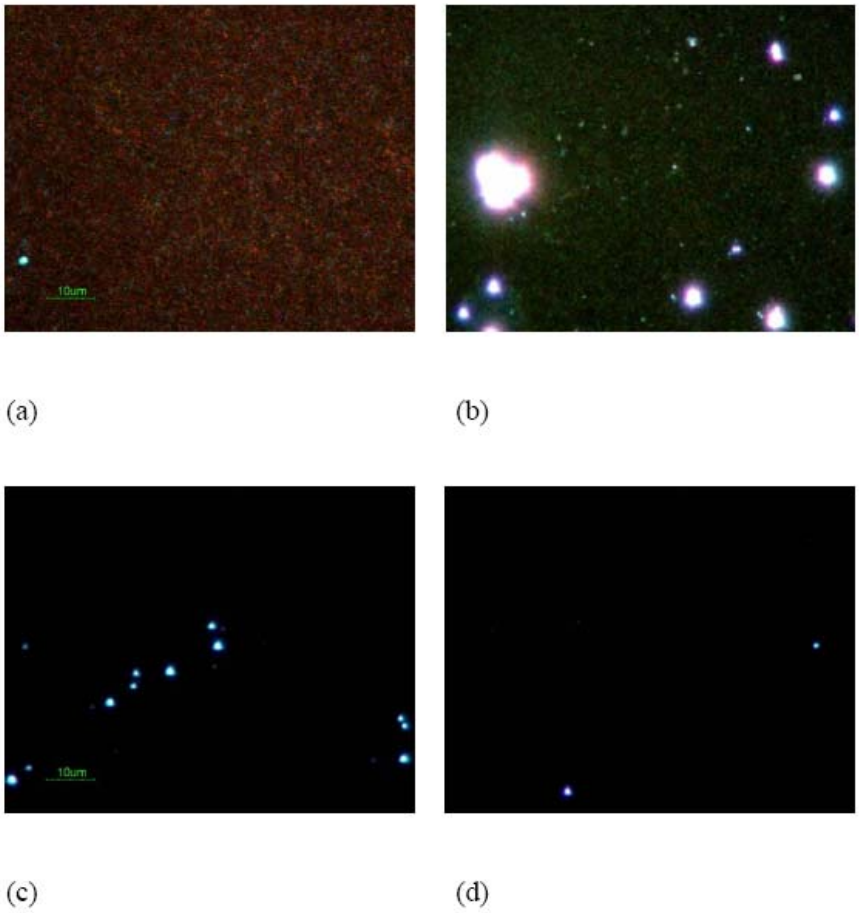

Figure 2.2 Optical microscopic dark filed images of Ag deposited on silicon (100) for different times of immersion. (a) immersion time: 60s; (b) 40s; (c) 20s; (d) 10s.

The process of electroless deposition indicates the mechanism of direct displacement reaction that results in the dissolution of Si by fluoride ions present in the solution with simultaneous reduction of Ag^+ ions on the Si surface by obtaining the electrons released by Si-H [4, 7, and 8]. The possible redox reaction for the Ag deposition on HF-treated silicon surfaces can be represented as:

$$4Ag^+ + Si(s) + 6F^-(aq) \rightarrow 4Ag(s) + SiF_6^{2-} \quad (3)$$

2.3.3 Particle Size and Roughness Measurement by AFM

The atomic force microscope (AFM) is an ideal tool for visualizing the surface size and for quantitatively measuring the nanometer scale surface roughness on many types of material surfaces. Advantages of the AFM for these applications are derived from the fact that the AFM has a very high three dimensional spatial resolution [9, 10].

Using Nanoscope III tapping mode AFM, surface data were obtained [1cm^2 Si (100) chip dipping in 4.9% HF + 0.8mM $AgNO_3$ for 20s].Shown in Figure 2.3, it is the section analysis of a silver deposited Si surface. In the small image in the left bottom, two red triangle tips indicate the diameter of one of the silver particles that is about 56.6nm. Line profile on the left top demonstrates that this particle is the middle size compared with others. It is estimated that the diameter of silver particles under this condition should be 50-100 nm. Because of the limitation of the software, we cannot obtain more information concerning particle size analysis.

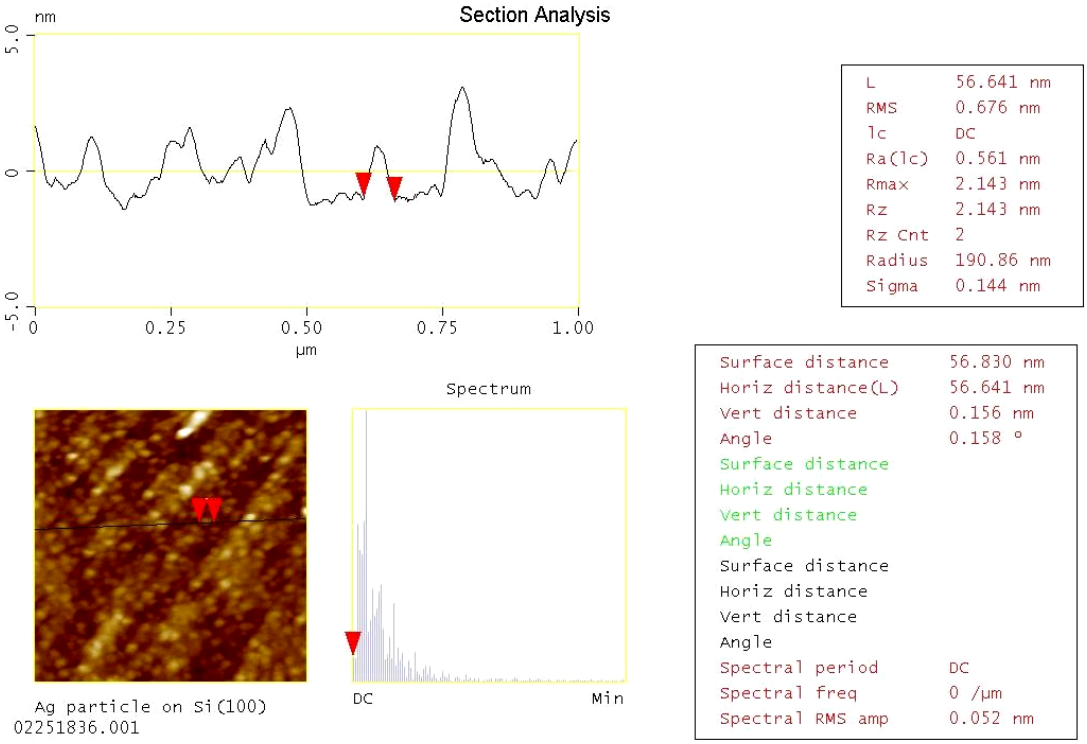

Figure 2.3 Section analysis of Ag deposited Si surface from AFM image.

Roughness is quantified by the vertical deviations of a real surface from its ideal form. If these deviations are large, the surface is rough; if they are small the surface is smooth. Roughness is typically considered to be the high frequency, short wavelength component of a measured surface [11].

For AFM measurements, the probe is commanded to scan over a two dimensional area on the surface. The spacing between data points may not be the same in both directions. Every roughness parameter is calculated using a formula for describing the surface. There are many different roughness parameters in use, but arithmetic average of absolute values roughness (R_a) is by far the most common. Besides R_a, here, we will apply another parameter that is the root mean square roughness (R_q) to describe surface roughness of silver deposition. The definition of Ra and Rq is listing below [12]:

$$R_{\mathrm{a}} = \frac{1}{l_{\mathrm{m}}} \int_{x=0}^{x=l_{\mathrm{m}}} |y| \, \mathrm{d}x \tag{4}$$

$$R_{\mathrm{q}} = \sqrt{\frac{1}{l_{\mathrm{m}}} \int_{x=0}^{x=l_{\mathrm{m}}} y^2(x) \, \mathrm{d}x} \tag{5}$$

Where l_m is evaluation length, x is distance coordinate along the measurement axis, and y is distance coordinate perpendicular to the measurement axis.

Figure 2.4 illustrates the surface morphology of Si (100) after hydrogen termination. From the image we can see that the R_q is from 0.6 to 1.0 nm and R_a is 0.6 to 0.8nm. The roughness is a little higher than reported Si (100) roughness, which is about 0.15nm [13]. After SC1, SC2 and HF etching treating, the surface of silicon is covered with hydrogen terminated and is hydrophobic.

Figure 2.5 illustrates the surface morphology after silver deposition. It shows that

roughness increased a lot. The R_q is from 1.4 to 1.5nm and R_a is from 1.1nm to 1.2nm. Compare to a cleaned Si (100) surface, both RMS and mean roughness increased 2 to 3 times.

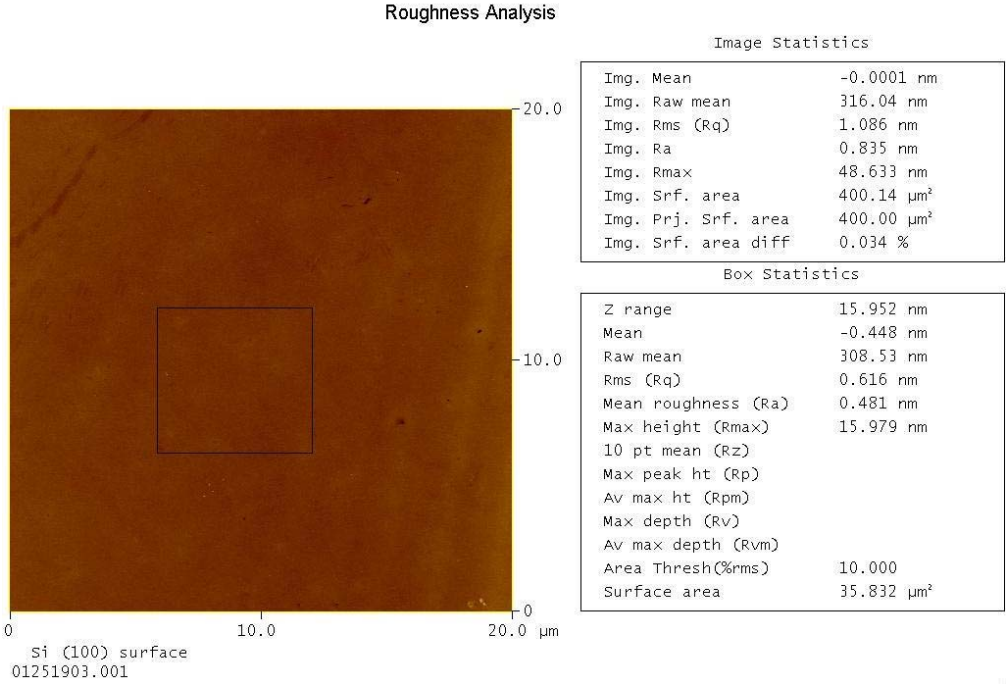

Figure 2.4 Roughness analysis of Si (100) AFM image after cleaning treatment.

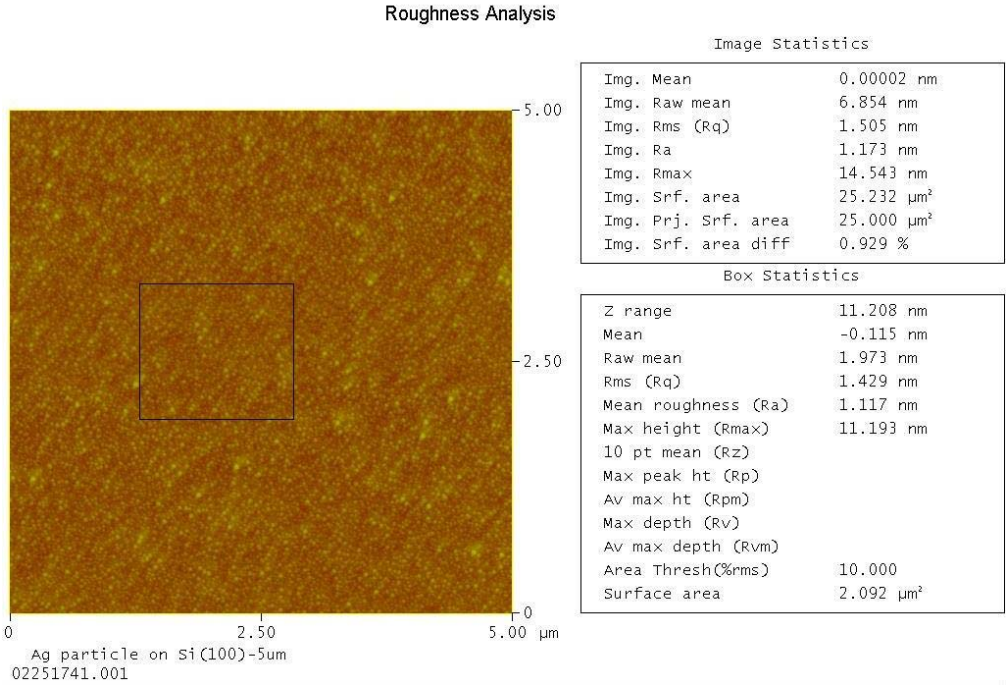

Figure 2.5 Roughness analyses of Ag nanoparticles on Si (100) from its AFM image.

2.3.4 IR Characterization of Ag/Si and SCN^-/Ag/Si Samples

Figure 2.6 shows IR results of various surface treatments between 1800 cm^{-1} and 2500cm^{-1}. A Si (100) ATR wafer after SC1 cleaning served as background surface. As described before, hydroxide formed on the surface of Si after SC1 treatment, as a result, Si after SC1 is also called HO-terminated Si and it is hydrophilic. Spectrum 3 is hydrogen terminated Si after 5min of 4.9% HF etching. The HF passivated Si surface demonstrates a complicated vibrational spectrum. The Si-H vibrational stretching frequency was observed in the region from 2050 cm^{-1} to 2150 cm^{-1}. The silicon dihydride (SiH_2) band exists at 2116 cm^{-1} [14]. The mono-hydride stretching modes are at 2088 and 2072 cm^{-1} corresponding to the coupled mono-hydride symmetric and asymmetric vibrational stretching frequencies. And the silicon trihydride is at 2138 cm^{-1}. Since Si (100) was used, the surface is di-hydride dominated. However, SC1 cleaning process caused small dents and holes on the surface of Si(100) that will have silicon mono-hydrides and trihydrides as shown in Figure 2.7.

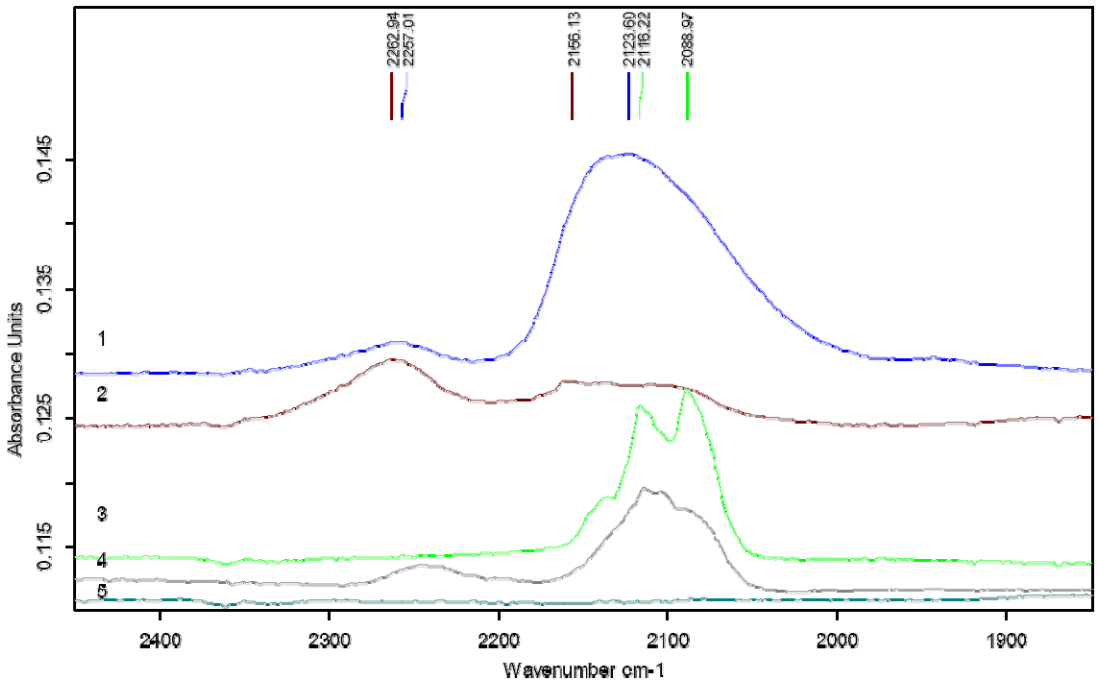

Figure 2.6 FTIR spectra of various surface treatments between 1800 cm^{-1} and 2500cm^{-1}.

Spectrum 1 (blue). SCN^- dipping on Ag particles;

Spectrum 2 (red). Ag deposit on H-terminated surface;

Spectrum 3 (green). H-terminated surface;

Spectrum 4 (grey). SCN^- dipping on H-terminated surface;

Spectrum 5 (indigo). SCN^- dipping on HO-terminated surface.

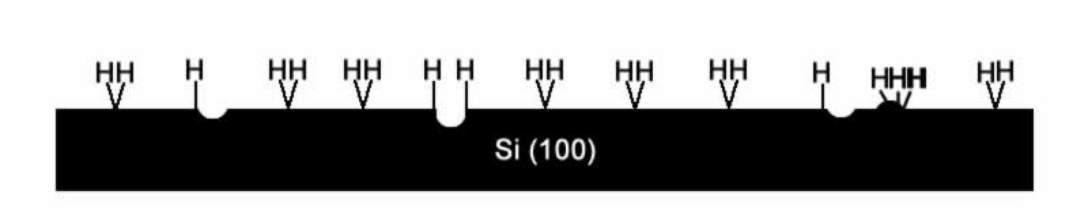

Figure 2.7 Schematic of hydride Si (100) surface.

Spectrum 2 shows H-terminated Si after Ag electroless deposition. A large amount of silicon hydride was eliminated from the surface, so IR peaks from 2050 cm^{-1} to 2150 cm^{-1} decreased and even disappeared with Ag deposition because of continuous reaction of Ag^+ with H-terminated Si surface. During the reaction as equation (3), Ag nano-particles were deposited continuously. IR absorption peaks of silicon hydride with back bonded oxygen (O_3Si-H) at the range from 2200 to 2300 cm^{-1} increased as the result of deposition. This IR area (2200 ~2300 cm^{-1}) becomes narrower during deposition and the center of the broad band shifts, demonstrating that the oxidation state of top layered Si was increasing. As well as Ag deposition reaction in equation (3), there is another surface oxidation reaction in which the surface of silicon atoms was attacked by H_2O. Figure 2.8 illustrates this reaction process below. A Si-Si bond is broken by the attack of two H_2O molecules. Adding the backboned oxygen weakens the Si-H and then -H is replaced by –OH, and the final oxidized product is O_3Si-H.

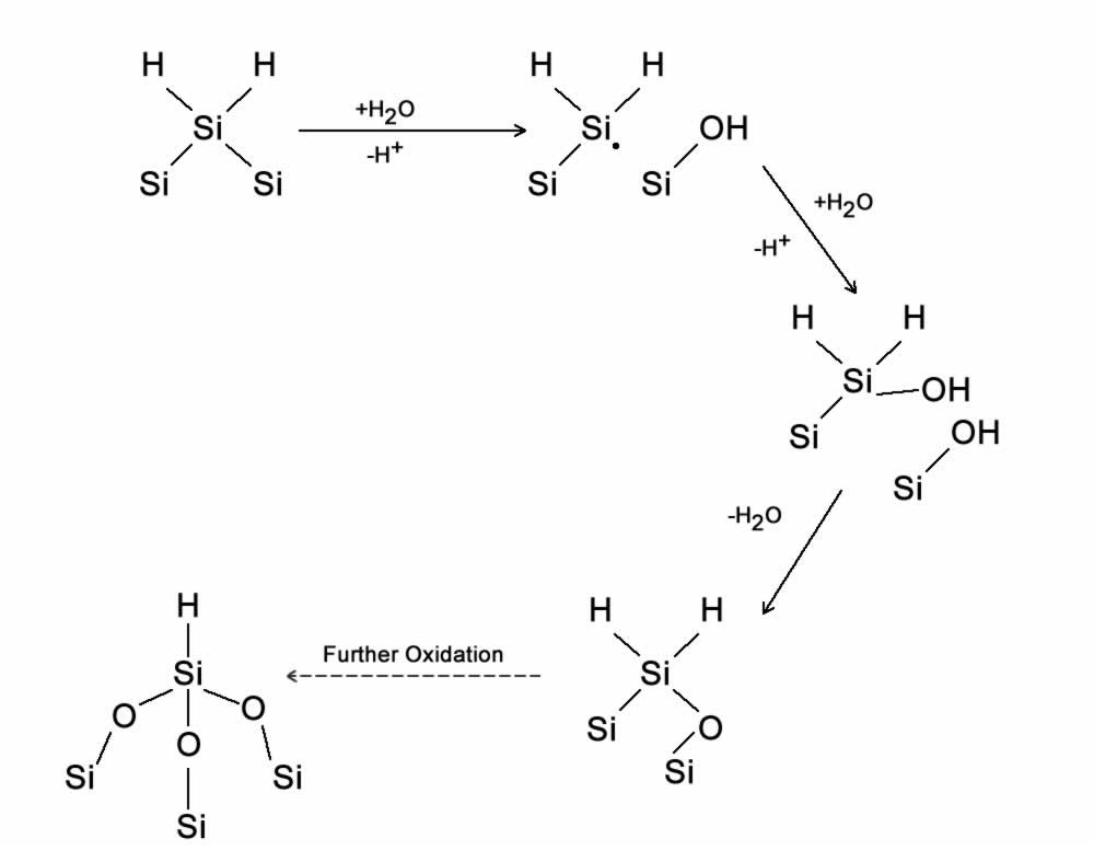

Figure 2.8 Schematic diagram of oxidation of Si (100) surface by injection of holes from metal ions.

Spectrum 1 from Figure 2.6 is a silver coating Si ATR wafer after in 5mM KSCN and 0.1M $KClO_4$ for 2 minutes. 2123 cm^{-1} board peak is stretch vibrational C=N bond from SCN^-, suggesting that SCN^- adsorbed through S atom on Ag electrode surfaces [4, 15-17].

2.4 Conclusion and Future Work

In this chapter, Ag nanoparticles electroless depositing on Si (100) surface has been proved and testified by microscope images, AFM images and ATR-FTIR analysis. SCN^- worked as an adsorbent to demonstrate the existence of Ag nanopartices, and this method was widely used and reported [4, 16]. However, due to the limitation of liquid adsorbent, SCN^- was easily contaminated or influenced by other ions in solution.

In order to overcome this, gas adsorbent such as CO and NO were introduced. As successful gas adsorbents and indicators [18, 19], CO and NO can be used to distinguish and measure Au, Ag, Cu and other metals or metal complex in surface science, catalyst and electrochemistry fields. Other simple structural gas molecules, like ethylene, also can work to evaluate catalyst ability of noble metals [19, 20]. Our next step is to apply these gas adsorbents to test catalyst properties of Ag nanoparticles.

2.5 Chapter References

[1]. "Plating." Wikipedia: http://en.wikipedia.org/wiki/Plating. Retrieved on March, **2009.**

[2]. "Electroless plating." Wikipedia: http://en.wikipedia.org/wiki/Electroless_plating. Retrieved on March, **2009.**

[3]. "Silver." Wikipedia: http://en.wikipedia.org/wiki/Silver. Retrieved on March, **2009**.

[4]. Huo, S.; Xue, X.; Li, Q.; Xu, S. and Cai, W. *J. Phys. Chem. B,* Vol. 110, No. 51, **2006.**

[5]. Chyan, O.; Chen, J. and Chien, H *J Electrochem. Soc.*, **1996,**143, 1.

[6]. Meyer, F. and White, J. *Semiconductor International*, Silicon Engineering Technology Center Laboratory, **1999**, July, 137.

[7]. Rodes, A.; Orts, J. M.; Perez, J. M.; Feliu, J. M.; Aldaz, A. *Elctrochem. Commun.* **2003**, 5, 56.

[8]. Delgado, J. M.; Orts, J. M.; Rodes, A. *Langmuir* **2005**, 21, 8809.

[9]. "Atomic Force microscope." Wikipedia: http://en.wikipedia.org/wiki/Atomic_force_microscope. Retrieved on March, **2009.**

[10]. Zavala, G. *Colloid Polym Sci*. **2008** 286:85–95

[11]. "Roughness." Wikipedia: http://en.wikipedia.org/wiki/Roughness Retrieved on March, **2009.**

[12]. Farshad, F. F.; Pesacreta, T. C. *Anti-Corrosion Methods and Materials.* **2003** 50: 6-60

[13]. Cotton, F.A.; Murillo, C.; *Advanced Inorganic Chemistry*, John Wiley & Sons; New York, **1999.**

[14]. Bateman, J. E.; Horrocks, B. R. and Houlton, A.; *J. Chem. Soc., Faraday Trans.,* **1997**, 93(14), 2427-2431

[15]. Weaver, M. J.; Barz, F.; Gordon, J. G., II; Philpott, M. R. *Surf. Sci.* **1983**, *125*, 409.

[16]. Hatta, A.; Sasaki, Y.; Suetaka, W. *J. Electroanal. Chem.* **1986**, *215*, 93.

[17]. Orozco, G.; Perez, M. C.; Rincon, A.; Gutierrez C. *Langmuir*, **1998**, 14, 6297-6306.

[18]. Kershen, K.; Celio, H.; Lee, I.; White, J. M. *Langmuir*, **2001**, 17, 323-328.

[19]. Hertwig, R. H.; Koch, W.; 1der, D. S.; Schwarz, H. *J. Phys. Chem.*, Vol. 100, No. 30, **1996**

[20]. Rojluechai, S.; Chavadej, S.; Schwank, J. W.; Meeyoo, V. *Catalysis Communications.* 8 (**2007)** 57–64

CHAPTER 3

PPATINA FORMATION STUDIES OF OXYGEN REDUCTION REACTION ON RUTHENIUM OR PLATINUM SURFACE

3.1 Introduction

Copper is the metal with a wide range of applications in all fields. Due to its high conductivity and affordable prices, it is the dominant material used in electrical power lines [1]. It has several other applications in electronic industries as well. Long time ago, copper has been employed in certain works of arts (monuments and sculptures) and in building constructions [2].

Figure 3.1 Statue of Liberty.

When a clean copper surface exposed to the atmosphere, its color will transform from shinning yellow-brown to a darkening brown and at last to an aesthetically green-blue. The top layer which caused the green-blue color is known as “patina” [3]. Patina can be found in many

outdoor architectures and statues. A definition for “patina” from the Merriam-Webster dictionary is “a usually green film formed naturally on copper and bronze by long exposure or artificially (as by acids) and often valued aesthetically for its color” [4]. Statue of Liberty is such a good example as shown in Figure 3.1. The process of transformation from copper to patina under natural atmosphere condition takes five to sixty years, however, in various experimental conditions; the time of patina formation is from couples of seconds to hours.

In general, patina is the name of a family of copper basic salts that can be detected from the outside green layer of aged copper in ambient. The representative formation of patina are $Cu_4SO_4(OH)_6$ (brochantite), $Cu_4SO_4(OH)_6 \cdot H_2O$ (posnjakite), and $Cu_4SO_4(OH)_6 \cdot 2H_2O$ (wroewolfeite) [5].

Scientists applied patina formation to study corrosion and protection of antiquity statues and deliberate decoration of arts or furniture. Others studied the structure and the forming mechanism of patina. In our study of electrochemical plating copper on noble metals, Dr. Yibin Zhang accidently revealed that patina formation occurred on the surface of platinum (Pt) or ruthenium (Ru) in a pH=5.0 $CuSO_4$ solution. In the follow-up research, the evidence implies that patina formation is related to oxygen reduction reaction [6].

Fuel cell is considered as a possible power source in future, which could be applied in automobiles and portable electronics. It is the answer to work out the energy shortage in nowadays and many countries invested a large amount of money to sponsor the related researches. Oxygen reduction reaction (ORR) is one of reactions in fuel cell and Pt is one of the most effective catalysts for ORR. However, the high price of Pt restricts its applications. To find an alternative high-performance catalyst is the popular research topics in recent years. Patina might work as an indicator to test the ORR activities in all sorts of materials.

In this chapter, electrochemical plating of Cu on the Ru/RuO_x and Pt electrode surface was studied in a pH=5.0 cupric sulfate ($CuSO_4$) solution. Compared to pH=0 solution, cyclic voltammetry (CV) diagram indicates a significant difference of electrochemical behaviors in solution pH=5. According to Dr. Yibi Zhang and Oscar's studies [6, 7], it is reported that an interesting posnjakite [$Cu_4SO_4(OH)_6 \cdot 2H_2O$] formation occurred during Cu plating. In this chapter, it is explained that this process was triggered by oxygen reduction reaction (ORR) on the Ru and Pt electrode surface. Cu_2O was found in the process. The mechanism of electrochemical reaction will be given and a proposed mechanism of forming $Cu_4SO_4(OH)_6 \cdot 2H_2O$ on Ru and Pt surface will be discussed.

3.2 Experimental

Ru disk electrodes were prepared by Ru shots (ESPI Inc.) form previously in the reported procedure. Potassium sulfate (K_2SO_4) (Aldrich) and $CuSO_4$ (Mallinckrodt) were used to make all electrolyte solutions in ultrapure water (18.2 MΩ Millipore). Electrochemical experiment was performed using CHI 760B (CH Instruments) potentiostat. A three-electrode cell with a Pt foil as the counter electrode (CE) and silver/silver chloride (saturate K_2SO_4) as the reference electrode was employed; all the potential, if not mentioned, reported in this paper is vs. the Ag/AgCl reference electrode.

Nikon ECLIPSE ME 600 optical microscope and Nikon DXM 1200 digital camera were used to observe and capture images from the surface of the Ru electrode. Nonoscope III Multimode SPM system (Veeco Inc.) was applied to scan the surface of the Ru wafer electrode after patination. An AFM tip was VISTA Probes™ non-contact tips (Nanoscience Instrument).

The rotating disk electrode system applied is the AFMSRX system from Pine Instrument.

Pt, Ru and glassy carbon (GC) RDE electrodes were used in 0.1M K_2SO_4 pH=5 solution to test their ORR activities.

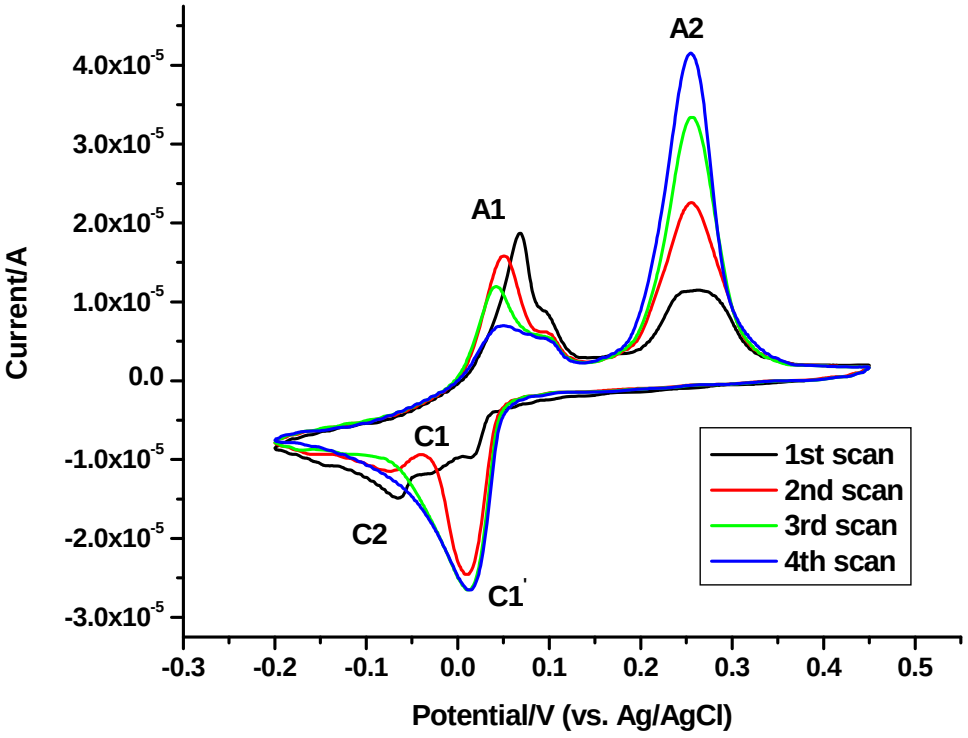

Figure 3.2 Cyclic voltammetry of polished Pt electrode in 2mM $CuSO_4$/0.1M K_2SO_4.

3.3 Results and Discussion

3.3.1 Cyclic Votammetry and Progressive Cyclic Voltammetry Experimental Results

Figure 3.2 illustrates cyclic voltammetry (CV) collected from a freshly polished Pt electrode in 2mM $CuSO_4$/0.1M K_2SO_4 solution in air. The pH was adjusted to 5.0 by adding 3.0M NaOH, The CV scans started from open potential cuicurt (OCP) of Pt, about 0.46V, and moved negative to let Cu^{2+} ions reductively deposit on the Pt surface.

On the cathodic range of the first scan, the first cathode shows up at -0.02V (C1), the second one at -0.07V (C2). On reverse anodic scanning, Cu species (Cu and Cu_2O) were

oxidized and stripping from the surface of the Pt electrode, the first anodic peak is at about 0.05V (A1), the second one at about 0.25V (A2). In the first CV scanning curve, there were well defined cathodic peaks, C1 and C2 as labeled in Figure 3.1, also two well defined anodic peaks A1 and A2. The interesting point is: with second, third and fourth CV scanning, C1 become bigger (labeled as C1' in diagram), C2 visually decreases (probablely a small C2 merge into the bigger C1); in anodic region, A1 keeps decreasing and A2 increasing.

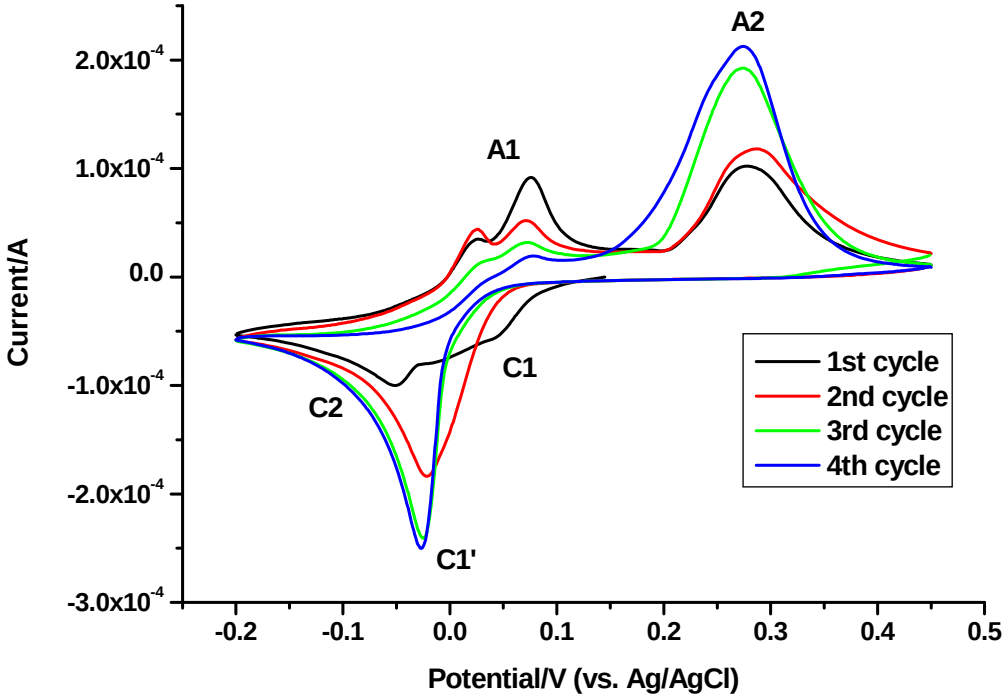

Figure 3.3 Cyclic voltammetry of polished Ru electrode in 2mM $CuSO_4$/0.1M K_2SO_4.

CV experiment of fresh polished ruthenium (Ru) in 2mM $CuSO_4$/0.1M K_2SO_4 solution shows the same tendency as CV of Pt, which is illustrated in Figure 3.3.

From Yibin Zhang's EQCM results [6, 7], the prediction of reaction for each CV peak is listing as following:

$$C1: \quad 2Cu^{2+} + 2e^- + 2OH^- = Cu_2O + H_2O \qquad (1)$$

C2: $Cu^{2+}+2e^{-}=Cu$ (2)

A1: $Cu=Cu^{2+}+2e^{-}$ (3)

A2: $Cu_2O + 2H^{+} = 2Cu^{2+} + H_2O + 2e^{-}$ (4)

$Cu^{2+} + 2OH^{-} = Cu(OH)_2$ (5)

These reactions could explain peaks from the first scanning cycle reasonably. However, both CV and EQCM of second scanning and afterward scans cannot be explained, because patina has formed with A2 reaction:

$3Cu(OH)_2 + Cu^{2+} + SO_4^{2-} + H_2O = Cu_4SO_4(OH)_6{\cdot}H_2O$ (6)

$Cu_4SO_4(OH)_6{\cdot}H_2O$ (posnjakite) is often formed from natural Cu corrosion process-patination. It is also a good technique for an artist to make a beautiful statute [8-12]. In this experiment, the mechanism is very similar to the Cu corrosion process [13]: at first, Cu_2O was formed in the atmosphere, then Cu_2O was oxidized to $Cu(OH)_2$. If there is SO_2 or SO_3 in the air, it will fall down combined with rain. At last the posnjakite will formed on the Cu surface. So one could conclude that the condition is similar to the one of chemical formation of posnjakite in the local area close to the electrode surface, it will be formed on the surface of the electrode [11, 12].

Oxygen is a key factor in affect in CV shape in pH=5.0 solutions. Oxygen reduction reaction (ORR) occured on the surface of the electrode as shown:

$O_2 + 2H_2O + 4e^{-} = 4OH^{-}$ (7)

This reaction causes the pH around the surface of the electrode (local area 25-30 μm adjacent to electrode) to increase [14]. It is reported that the local pH can reach 10 to 12 in aerated NaCl due to ORR by using the electrochemical pH microsensor [15]. We believe the local pH increase is the trigger to form Cu_2O because the thermodynamically favored reduction process is the Cu metal at low pH as listed in equation (2). At higher pH, the formation of Cu_2O

would be favored as shown in equation (1) [16, 17]. Figure 3.4 is the picture to show how to form Cu_2O in local area of electrode.

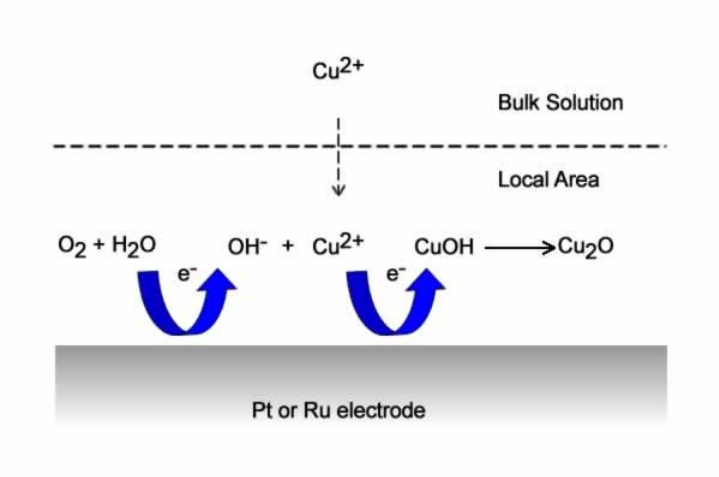

Figure 3.4 Cu_2O formations in the local area of Pt or Ru electrode.

Local pH increase caused by ORR is very important for Cu_2O formation. Lee reported that their group can get Cu_2O in pH 4.7 solutions [18]. He speculated because local pH increases due to equation (1). In our study, this point was confirmed by Zhang and Oscar's conclusions [6, 7] and progressive CV graph from Figure 3.5.

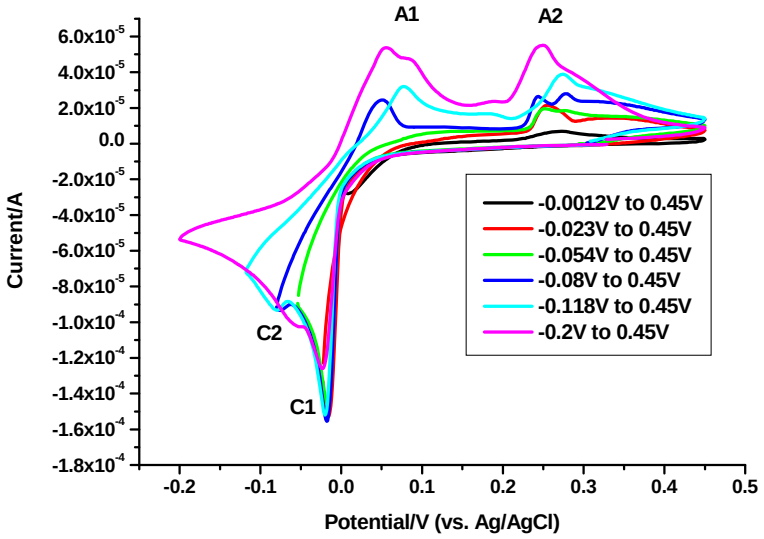

Figure 3.5 Progressive CV of Ru electrode in 2mM $CuSO_4$/0.1M K_2SO_4 pH=5 solution.

Figure 3.5 illustrated progressive CV cycles with different working windows. They all

used fresh polished Ru electrodes in 2mM $CuSO_4$/0.1M K_2SO_4 pH=5 solution. Comparing the first three (black, red and green curves) with other scan cycles, one can clearly conclude that the C1 peak is related to A2 and that C2 is related to A1 [6, 7], There is no C1 peak but an obvious C2 at the cathodic region and a huge A1 peak at the anodic region. This is strong evidence that C1 is the Cu_2O formation reaction while A2 is the $Cu_2O/Cu(OH)_2$ reaction peak, and C2 and A1 are Cu formation and stripping peaks.

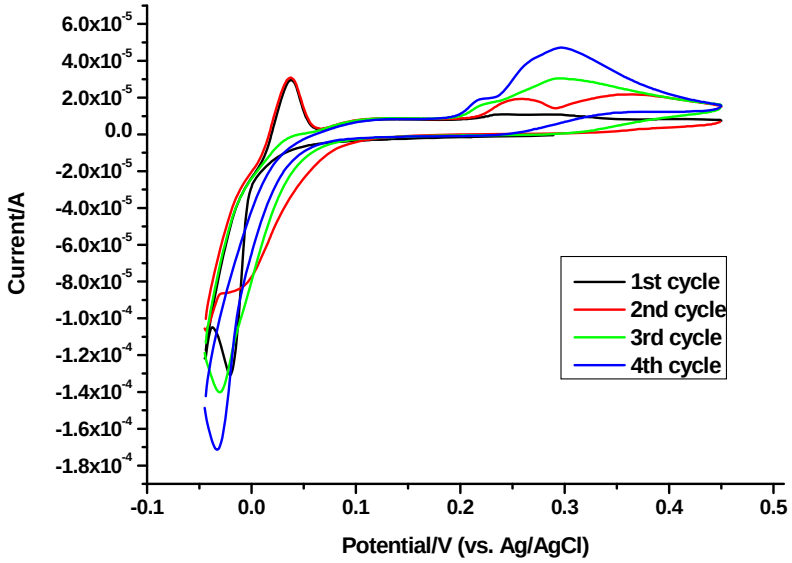

Figure 3.6 CV of Ru in 2mM $CuSO_4$/0.1M K_2SO_4 from -0.05 to 0.45V (vs. Ag/AgCl).

Figure 3.6 shows the situation after continuous CV scans. The experiment condition is similar to previous experiment: polished Ru electrodes in 2mM $CuSO_4$/0.1M K_2SO_4 (pH=5) solutions run four cycles of CV and the working window is from -0.045V to 0.45V (vs. Ag/AgCl). From the graph, the first two cycles (black and red curves) are different from the last two cycles (green and blue curves) since the surface condition of the electrode has changed during the experiment. At first the surface is fresh Ru, so ORR, Cu_2O formation and Cu formation occur at the cathodic region. However, the reduced end of CV is only -0.045V, it

would form large amounts of Cu_2O while forming small amount of Cu. According to the EQCM conclusion [6, 7], the cathodic peak in the 3rd and 4th cycle is no longer C1 (Cu_2O formation) and C2 (Cu formation) but patina dissolve peak, which is labeled as C1'. This experiment explained what would happen when Cu_2O/Cu^{2+} reactions dominated. A large amount of patina would form in the C2 area and certainly Cu/Cu^{2+} became less and less.

In an opposite way, when only Cu/Cu^{2+} reactions occurred, what would happen? Figure 3.7 and Figure 3.8 provided us with information. They are results of a stirring solution experiment, which applied Ru electrode in 2mM $CuSO_4$/0.1M K_2SO_4 (pH=5) solutions. Stirring the solution would create a homogenous solution environment. To express it exactly: in this experiment, convection (by stirring) would keep the pH value at 5.0 even in the local area. In that case, Most of Cu^{2+} are reduced to Cu in the local area since Cu^{2+} ions are sufficient by stirring effect.

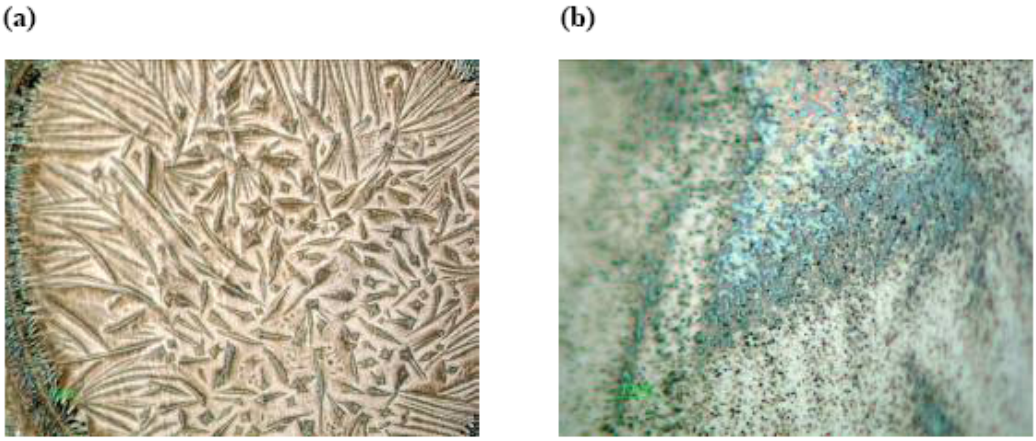

Figure 3.7 Optical microscope images of Ru electrode in stirring effect. (a) 50× magnification; (b) 1000× magnification.

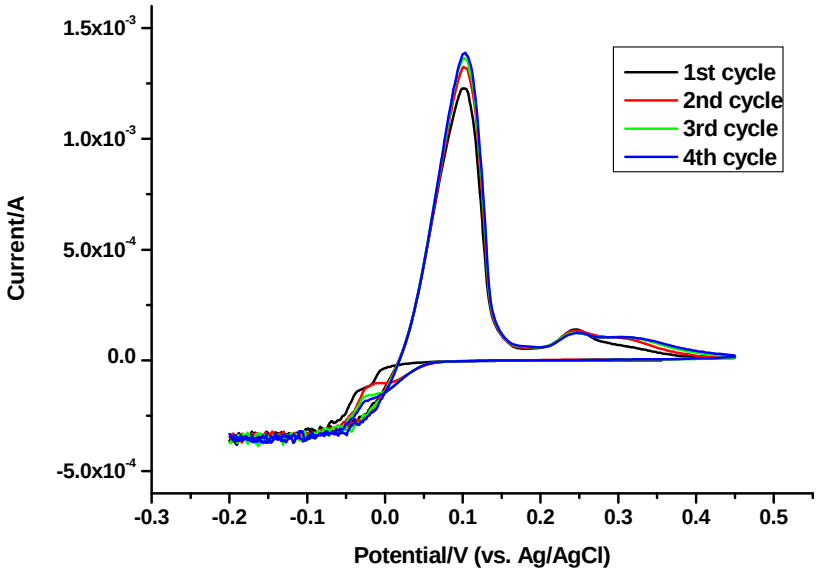

Figure 3.8 CV of Ru in stirring 2mM $CuSO_4$/0.1M K_2SO_4 solution.

Due to stirring the solution, Cu^{2+} would keep reducing to Cu and Cu/Cu^{2+} reactions took the major place. However, stirring cannot totally remove oxygen, so it is still had little Cu_2O formed by ORR. In the cathodic area, it is hard to see C1 and C2 peaks from Figure 3.8 because of stirring, and correspondingly, huge A1 (Cu stripping) and small A2 (Cu_2O/CuOH) peaks could be predicted. Microscope images of Figure 3.7 confirm that both Cu and Cu_2O exist on the surface of electrode because one can see the similar morphology of Cu and Cu_2O deposition. See more detailed discussion on section 3.3.2.

3.3.2 Analysis of Optical Microscope and AFM images

Optical microscope and AFM images can provide a direct view of morphological change of the electrode surface. By observing and analyzing the surface of the electrode, one can have an intuitive idea of reactions.

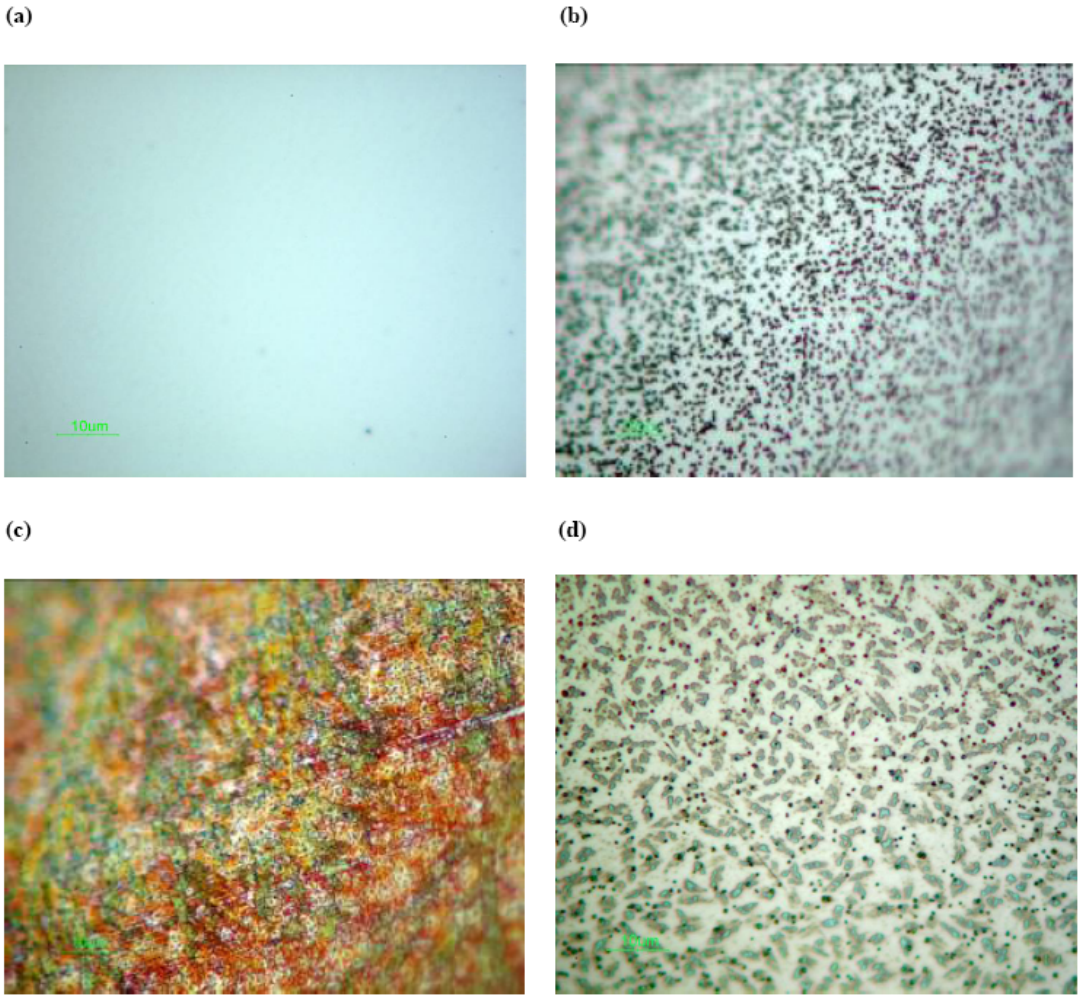

Figure 3.9 Optical microscope images of Ru electrode. (a) Fresh polished; (b) C1 reaction (Cu_2O formation); (c) C2 (Cu and Cu_2O formation); (d) A2 (patina formation).

Different Ru electrodes in various reactions were shown in Figure 3.9. The images begin with a cleaned and polished Ru surface [Figure 3.9 (a)]. Next, a C1 reaction caused Cu_2O formation on the surface, which shows as many small black cubic dots as shown in Figure 3.9 (b). The Cu_2O cubic structures are not good conductors. Once they were formed, the black dots are difficult to remove by electrochemical methods. During the C2 reaction, both Cu (as red and brown color) and Cu_2O (as black cubic dots) existed on the surface, which is shown in Figure 3.9 (c). Even after patina formation [Figure 3.9 (d)], certain Cu_2O dots were still observed and green-blue patina grew in the surrounding of Cu_2O dots.

Figure 3.10 illustrates the AFM image of Cu_2O on Ru surface. According to the image, a cubic structure of Cu_2O blocks is easily identified from other particles. The size of most Cu_2O cubes is around 0.5μm×0.5μm, which is very close to the literature reported.

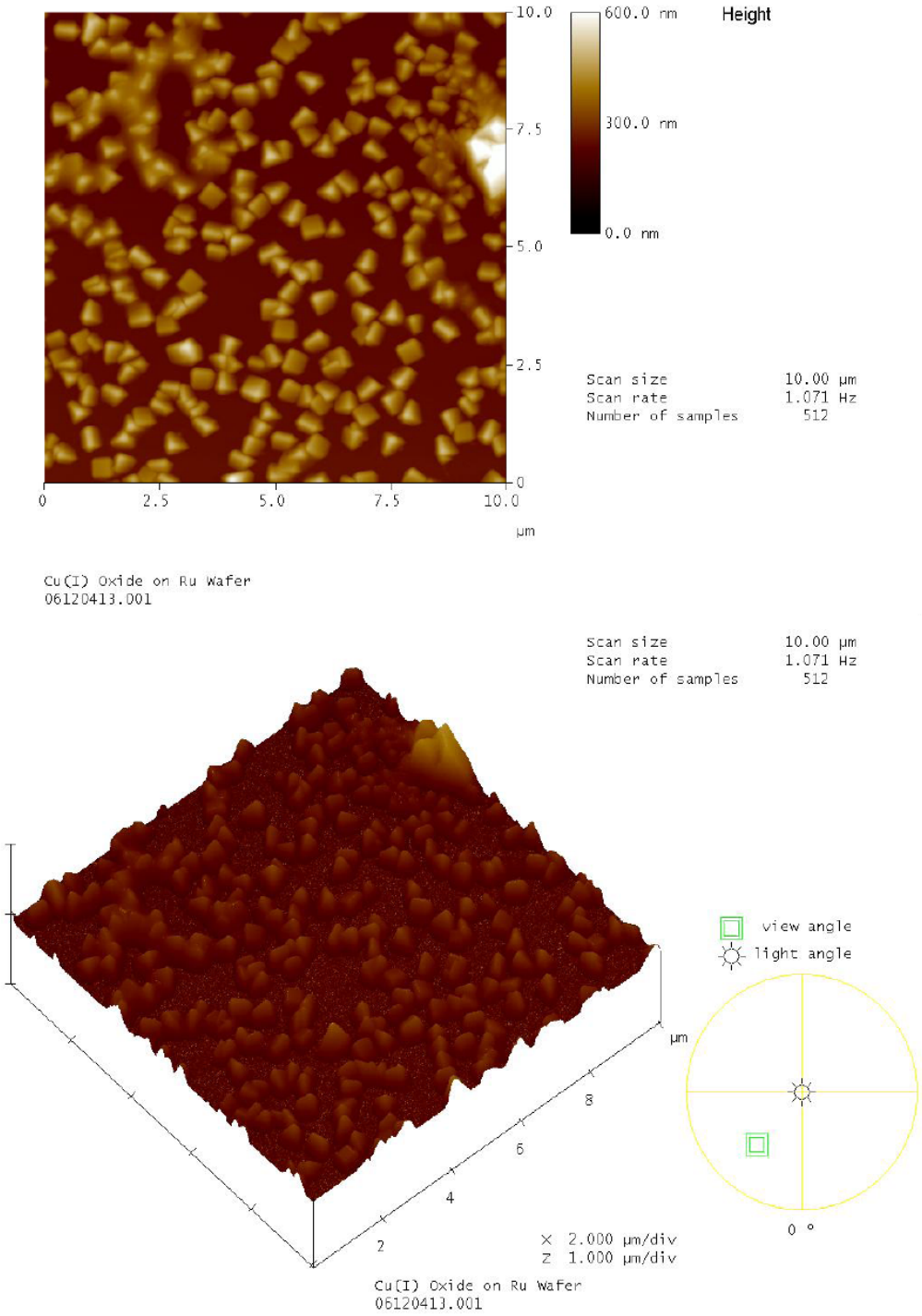

Figure 3.10 AFM images of Cu_2O formation (hold potential at C1 peak).

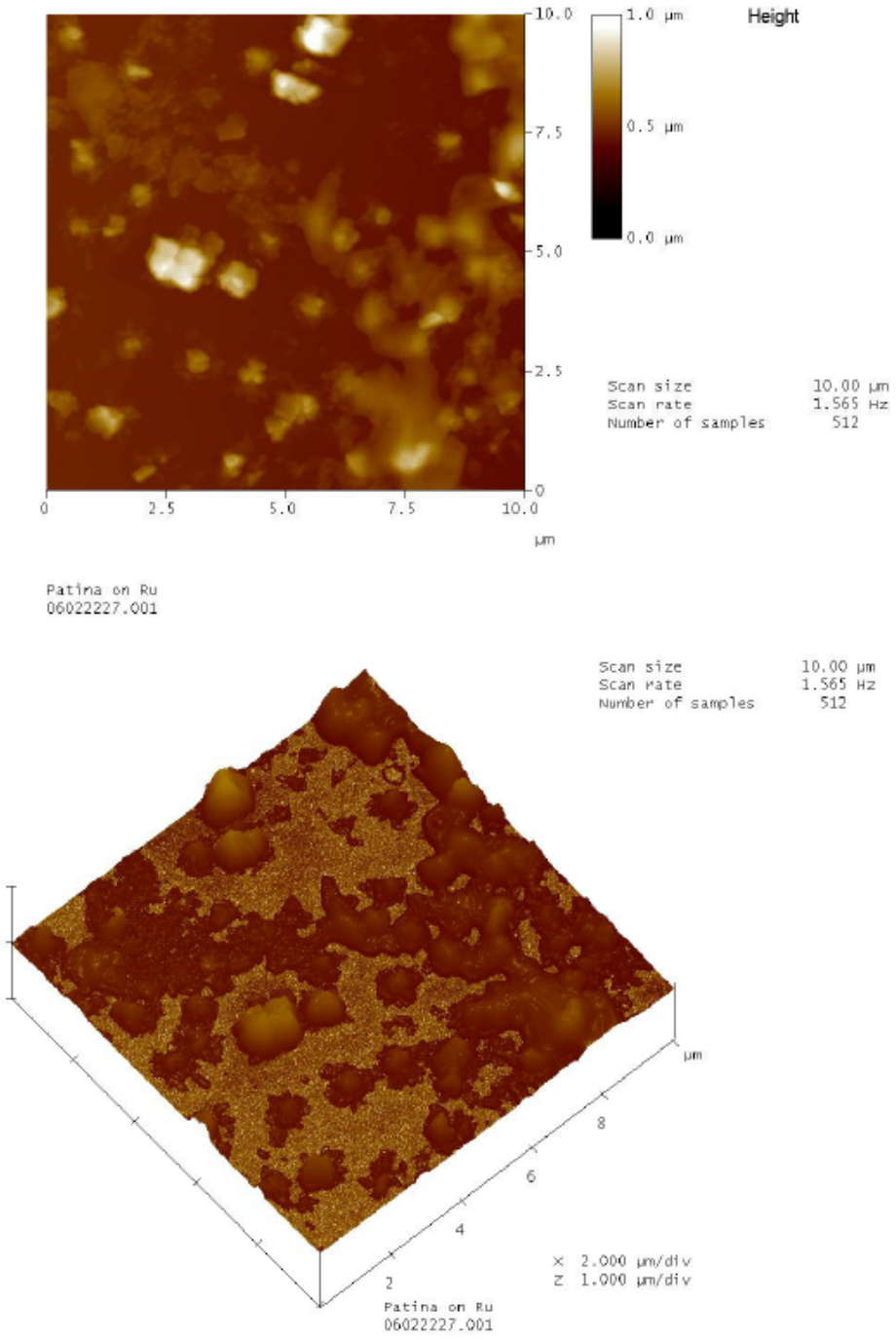

Figure 3.11 AFM images of patina formation (hold potential at A2 peak).

AFM images shown as Figure 3.11 provide us with more information about patina formation under 10µm scales. From AFM images, Cu_2O as a cubic like structure could be easily

identified and patina like mash potatoes could be seen around Cu_2O. However, most Cu_2O were not the sharp cubic since after A2 reaction, patina formed from Cu_2O and the original Cu_2O structure was destroyed. In addition, patina was only generated around Cu_2O which is additional evidence that patina comes from Cu_2O.

3.3.3 Pourbaix Diagram of Patina

Pourbaix diagrams, also called potential/pH diagrams, demonstrate equilibrium phases of an aqueous electrochemical system by math simulation [19]. The vertical axis is labeled as E for the potential with respect to the standard hydrogen electrode (SHE) as calculated by the Nernst equation. The horizontal axis is labeled pH. In addition, temperature and concentration of solvated ions in solution will shift the equilibrium lines in accordance with the Nernst equation. Temperature and concentration of active ions will influence the equilibrium lines from calculation.

Figure 3.12 are pourbaix diagrams that indicate the relationship between potential and pH less than 2mM $CuSO_4$/0.1M K_2SO_4 solution. From Figure 3.12(a), it can predicted that when pH>4.5, Cu_2O will form and patina will form when pH>5.2. Arrows in Figure 3.12(b) simulate and explain reactions during CV scanning. Red arrows show the cathodic direction when reduction reactions occur. It starts from OCP of Ru electrode at pH=5, and when ORR happened, the local area of electrode surface sharply increased. Cu_2O would be formed first as a C1 peak in the CV diagram. Since the reaction of Cu_2O formation consumed OH^-, the local pH would decrease and it would enter the area to form Cu, which demonstrated as C2 in CV.

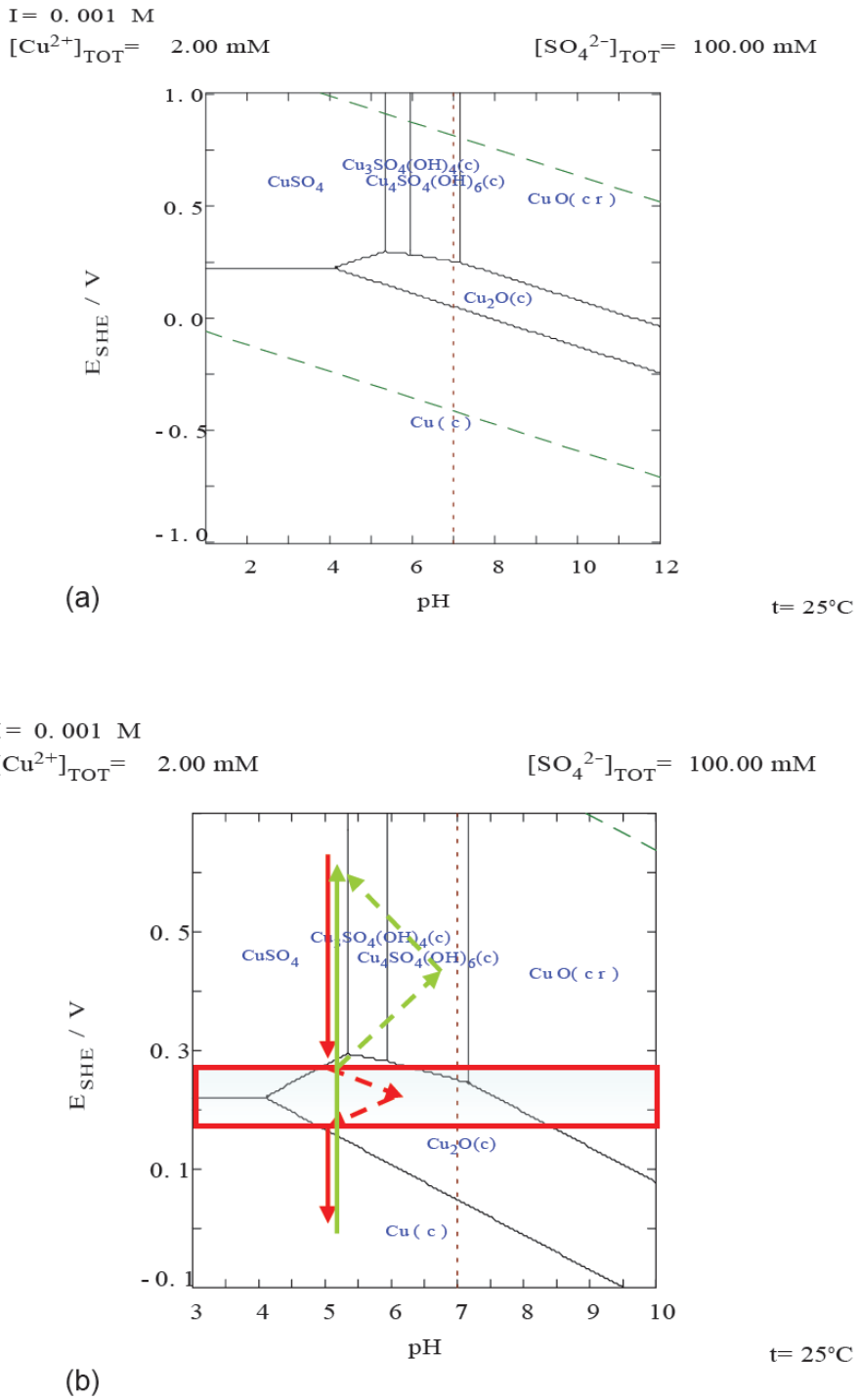

Figure 3.12 Pourbaix diagrams of 2mM $CuSO_4$/0.1M K_2SO_4 solution.

Anodic process (green arrows) is a similar process. From -0.02V to 1.8V, Cu is oxidized to Cu^{2+}, which is a Cu stripping process and it is the A1 peak in CV of the Ru or Pt electrode. Then,

equation (4) and (5) occur as shown as the A2 peak. Since Cu_2O is not a fine conductor, it will postpone the oxidation of Cu_2O, thus the A2 peak apart from A1 can be explained. Local pH will increase, shown in equation (4), which triggered the patina formation as shown in equation (6). In Pourbaix diagrams, increasing pH will result in reactions prefer to form $Cu_3SO_4(OH)_4$ and $Cu_4SO_4(SO)_6$, which coincides with the CV result.

3.3.4 Rotating Disk Electrode (RDE) Experimental Results

Using Pt, Ru, and GC (glassy carbon) electrodes respectively, I ran CV or LSV (Linear Sweep Voltammetry) in 0.1M K_2SO_4 solution under various rotation speeds from 0 to 3600rpm. The data of current were collected at ORR area, and then the plot was draw by square root of rotating speed versus current to analyze their slopes.

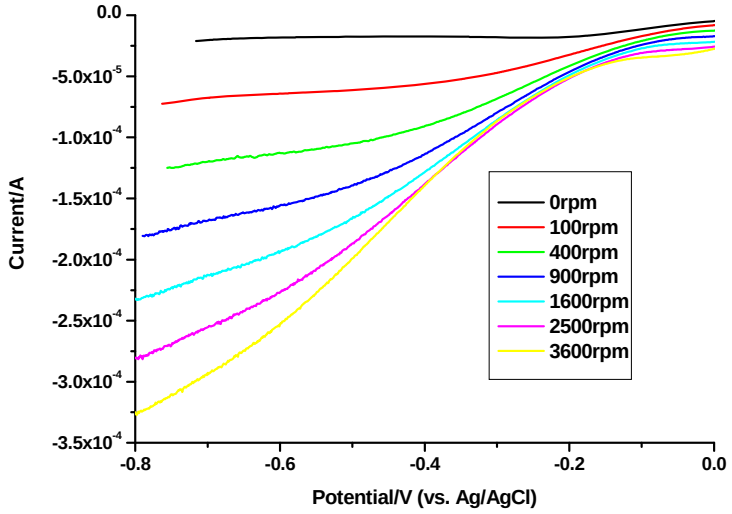

Figure 3.13 LSV of Ru in 0.1M K_2SO_4, pH=5 under various rotating rates.

Figure 3.13 is the LSV results of Ru in 0.1M K_2SO_4, pH=5 under different rotating speeds. The ORR area of Ru is about -0.2V to -0.8V (vs. Ag/AgCl). The LSV diagram shows that higher speed rates brought much more negative current because high rotating rates increase the mass

transfer on the surface of electrodes. Pt has the same behavior as Ru since both of them are ORR active metals. However, GC is an inert material of ORR, so its CV varies from Pt and Ru under this condition.

According to the Levich equation [20], showing as equation (8), the plot of j_L vs $\omega^{0.5}$ is linear:

$$j_L = 0.62nFD^{0.67}\nu^{-0.166}c\omega^{0.5} \quad (8)$$

Where j_L is the current density; n is the number of electrons involved in electrode reaction; F is the Faraday constant, 96,500 C·mol^{-1}; D is the diffusion coefficient; ν is the kinematic viscosity; c is the concentration of electro-active species in bulk solution; and ω is the rotation speed.

In this RDE experiment, the size of electrodes are the same, the solution is the same, so current here can represent current density in equation (8), and the slopes of plots in Figure 3.13 are proportional to D. In other words, materials which have higher slopes will demonstrate good ORR activities.

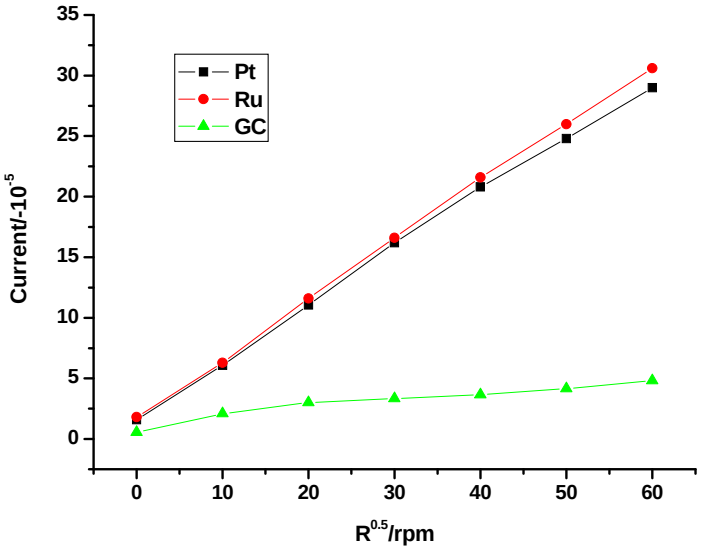

Figure 3.14 Diagram of square root of rate ($R^{0.5}$) vs. current for Pt, Ru, and GC.

Coinciding with our predictions and as previously reported, Pt and Ru metals are active ORR materials but GC is not. In this case, patina formation of GC is small as shown in Figure 3.15.

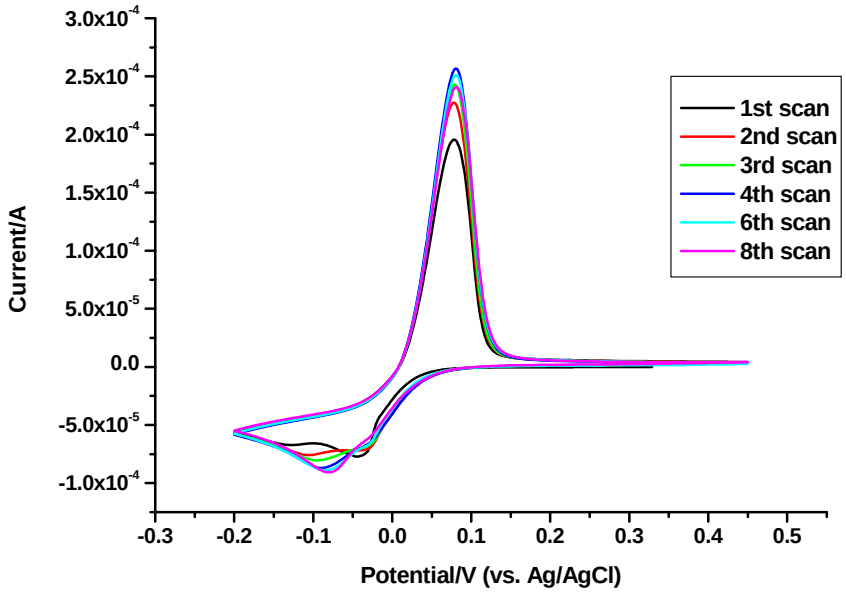

Figure 3.15 Cyclic voltammetry of glassy carbon (GC) electrode in 2mM $CuSO_4$/0.1M K_2SO_4, pH=5 solution.

3.3.5 Test ORR of Electrochemical Oxidized Ru Using Patina Formation Method

In this experiment, patina formation was applied to identify ORR on the electrochemical oxidized Ru surface.

As discussed above, patina formation can be labeled as a sign of the occurrence of oxygen reduction reaction (ORR). Can patina formation be used to test ORR activity for certain metals or metal oxidizes? The answer is yes. Electrochemical oxidized Ru is such an example.

Electrochemical oxidized Ru could be prepared in either an acidic medium or an alkali medium. According to J. Juodkazyte's paper [21, 22], a series of electrochemically oxidized Ru surfaces produced in 0.5M H_2SO_4 are as follows: formation of $Ru(OH)_3$ takes place at 0.2

V<E<0.8 V (vs. RHE); formation of $RuO_2 \cdot nH_2O$ at 0.8 V<E< 1.1 V (vs. RHE) and at 1.1 V<E<1.4 V (vs. RHE) passivation of Ru electrodes takes place to form anhydrous RuO_2. Both $Ru(OH)_3$ and $RuO_2 \cdot nH_2O$ are reversible ruthenium oxide, which means these oxides could be reduced back to Ru metal. Nevertheless, RuO_2 is irreversible because Ru oxides are hard to reduce to Ru.

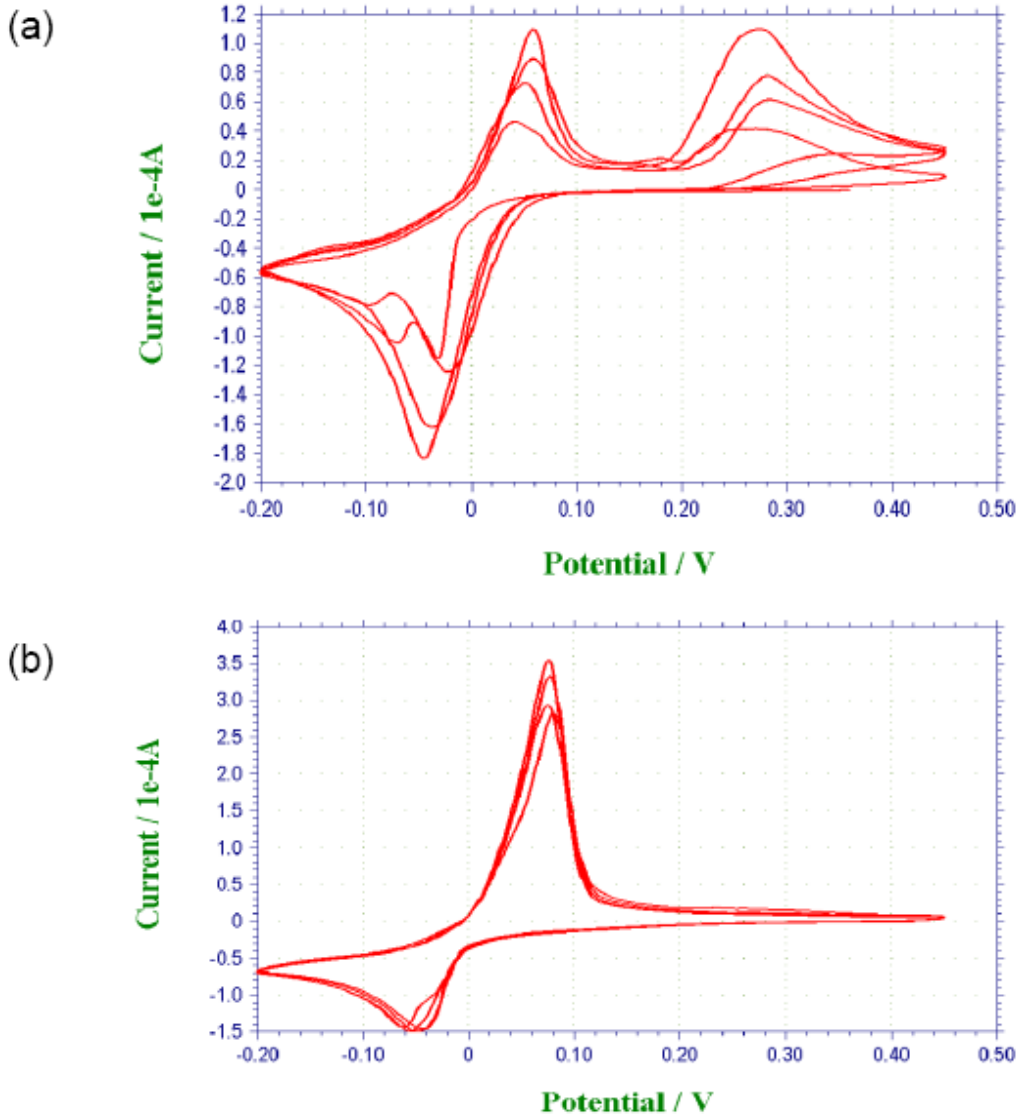

Figure 3.16 (part one) Cyclic voltammetry of Ru and reversible ruthenium oxides electrodes in 2mM $CuSO_4$/0.1M K_2SO_4, pH=5 solution. (a) Polished Ru; (b) Ru oxides made by holding Ru in 0.5M H_2SO_4 for 0.6V, 100s.

(c)

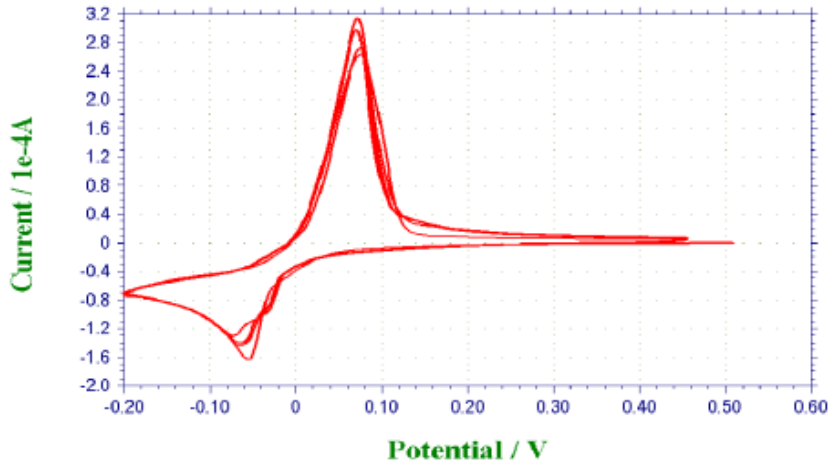

(d)

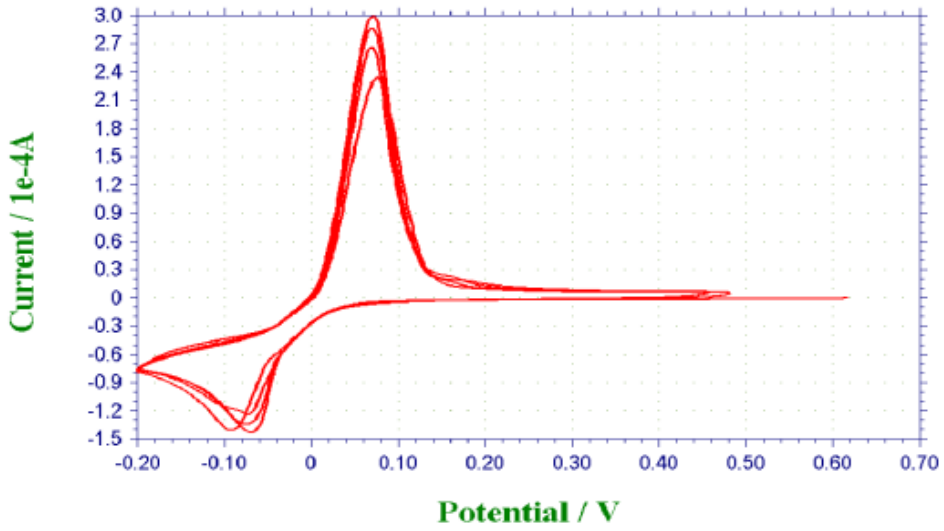

Figure 3.16 (part two) Cyclic voltammetry of Ru and reversible ruthenium oxides electrodes in 2mM $CuSO_4$/0.1M K_2SO_4, pH=5 solution. (c) Ru oxides made by holding Ru in 0.5M H_2SO_4 for 0.8V, 100s. (d) Ru oxides made by holding Ru in 0.5M H_2SO_4 for 1.0V, 100s.

Fresh polished Ru shot electrodes were kept at 0.6V, 0.8V, and 1.0V (vs. Ag/AgCl) in 0.5M H_2SO_4 for 100s respectively. Then a CV was ran using treated Ru electrodes under 2mM $CuSO_4$/0.1M K_2SO_4, pH=5 solution. Comparing CVs with a freshly polished Ru electrode, the result, which is illustrated in Figure 3.16, indicates that no ORR happened in electrochemical oxidized Ru surface. This is shown by little or no patina formation peak in the CV diagram. Ruthenium oxides in Figure 3.16 (b), (c) and (d) are $Ru(OH)_3$. The result of CV for reversible Ru

oxides depicts that ORR is very unlikely to happen on the surface of reversible Ru oxides.

3.4 Conclusion and Future Work

In this chapter, the patina formation experiment is designed to demonstrate that it could be a useful tool to identify oxygen reduction reactions. The relationship among ORR, Cu_2O formation and patina formation is well discussed and illustrated by a series of experiments of progressive CV, optic microscope images, AFM images, Proubaix simulation diagrams and RDE analysis. Furthermore, patina formation method is applied to test ORR activity of various Ru oxides. Other type of metals and materials could be tested in the same way to trace ORR in future.

The purpose of this patina experiment is to design a low-cost and easy-operating method to tell the ORR activity of materials. Compared with searching the ORR peak directly from CV diagram, patina formation is obviously to find and distinguish. Before apply rotating disk electrode system to estimate and calculate the basic hydrodynamic parameter, patina formation reaction might label the ORR qualitatively.

However, this method is only applied in pH=5.0 solution. Results from solutions with other pH ranges are hard to predict. Other metal basic salts [23-26] may be the indicators to discuss ORR reactions in other pH range. For example, in J. Génin's paper [24], the mechanism of forming green rust (groups of iron basic salts) has been well studied. This green rust formation, as the same as the patina formation, might identify ORR in the range from pH 6 to pH 7. In my future work, I will focus on iron basic salts and zinc basic salts testing experiments and I will determine several metal basic salts to identify ORR in broader pH range solutions.

3.5 Chapter References

[1]. "Copper." Wikipedia: http://en.wikipedia.org/wiki/Copper. Retrieved on March, **2009**.

[2]. Noli, F.; Misaelides, P.; Hatzidimitriou, A.; Pavlidou, E. and Kokkoris, *M. J. Mater. Chem.,* **2003**, 13, 114-120

[3]. Fitzgerald, K. P.; Nairn, J. and Atrens, A. *Corrosion Science*, Vol. 40, No. 12, pp. 2029-2050, **1998**

[4]. "Patina" Merriam-Webster on-line dictionary; http://www.merriam-webster.com/ Updated by March, **2009**

[5]. "Patina." Wikipedia: http://en.wikipedia.org/wiki/Patina. Retrieved on March, **2009.**

[6]. Zhang, Y.; Venkataraman, S.; Chyan, O. "Investigation of electrochemical copper patination on noble metal surfaces" Abstracts of Papers, 231st ACS National Meeting, Atlanta, GA, United States, March 26-30, **2006**

[7]. Zhang, Y.; Ojeda, O.; Flores, S.; Arunagiri, T.; Chyan, O. "Study of Cu Complex Formation on the Ruthenium Surface using Cyclic Voltammetry and X-ray Photoelectron Spectroscopy" Abstracts, 60th Southwest Regional Meeting of the American Chemical Society, Fort Worth, TX, United States, September 29-October 4 (**2004**)

[8]. Christy, A.G.; Lowe, A.; Otieno, V.; Otieno-Alego, V.; Stoll, M. and Webster, R.D. *Journal of Applied Electrochemistry* 34: 225-233, **2004**

[9]. Veleva, L.; Quintana, P.; Ramanaluskas, R.; Pomes R. *Electrimica, Acta*, 41(10) 1641-1646 (**1996**)

[10]. Malvault, J. Y and Lopitaux, J. *Jounal of Applied Electrochemistry* 25(**1995**) 841-845

[11]. Schlesinger, R.; Klewe-Nebenius H. and Bruns, M. *Surface and Interface Analysis* 30, 135-139 (**2000**)

[12]. Noil, F.; Misaelides, P.; Hatzdimitriou, A.; Pavlidou E. and Kokkorris, M. *J. Mater. Chem*. **2003**, 13, 114-120

[13]. CiCileo, G. P.; Grepo, M.A.; Rosales, B.M. *Corrosion Science* 46 (**2004**), 929-953.

[14]. King, F.; Quinn, M.J.; Like, C.D. *Journal of Electroanalytical Chemistry* 385(**1995**) 45-55

[15]. Hartinger, S. and Doblhofer, K. *Journal of Electoanalytical Chamistry*, 380(**1995**) 185-191

[16]. Switzer, J.; Huang, C.; Huang, L.; Miller, F.; Zhou, Y.; Raub, E.; Shumsky M.; and Bohannan, E. *J. Mater. Res*, Vol. 13(4) 911-916(**1998**)

[17]. Huang, L.; Bohannan, E.; Huang, C. and Switzer, J. *Israel Journal of Chemistry* Vol. 37 **1997** p293-301

[18]. Lee, J. and Tak, Y. *Electrchemical and Solid- State Letter*. 2(11) 559-560 (**1999**)

[19]. "Pourbaix diagram." Wikipedia: http://en.wikipedia.org/wiki/Pourbaix_diagram. Retrieved on March, **2009.**

[20]. Nikolic, J.; Expósito, E.; Iniesta, J.; González-García, J. and Montiel, V. *Journal of Chemical Education*. Vol. 77 No. 9 September **2000**

[21]. Juodkazyte, J.; Vilkauskaite, R.; Stalnionis, G.; Sebeka, B.; Juodkazis, K. *Electroanalysis* 19, **2007**, No. 10, 1093 – 1099

[22]. Sugawara, Y.; Yadav, A.; Nishikata, A. and Tsuru, T. *Journal of Electrochemical Society*, 155 (9) B897-B902 (**2008**)

[23]. Simon, L.; Genin, J. and Refait, P. *Corrosion Science*, Vol. 39, No. 9, pp. 1673-1685, **1997**

[24]. Génin, J.; Ruby, C.; Géhin, A.; Refait, P. *C. R. Geoscience.* 338 (**2006**) 433–446

[25]. Lee, C.; Qina, Z.; Odziemkowski, M.; Shoesmith, D. *Electrochimica Acta* 51 (**2006**) 1558–1568

[26]. Peulon, S. and Lincot, D. *J. Electrochem. Soc.,* Vol. 145, No. 3, March **1998**

COMPLETE REFERENCE LIST

"Atomic Force microscope." Wikipedia: http://en.wikipedia.org/wiki/Atomic_force_microscope. Retrieved on March, **2009**.

Bard, A.J.; Faulkner, L.R. *Electrochemical Methods: Fundamentals and Applications***.** New York: John Wiley & Sons, 2nd Edition, **2000**

Barnaby J. F. "Regulators Stamp Copper as a Germ Killer." http://www.nytimes.com/2008/03/26/business/26microbes.html?_r=1&scp=2&sq=copper&st=nyt&oref=slogin. *New York Times*. March 26, **2008**.

Bateman, J. E.; Horrocks, B. R. and Houlton, A.; *J. Chem. Soc., Faraday Trans.,* **1997**, 93(14), 2427-2431

Bertolini, J.C. *Journal of Emergency Medicine*, Vol. 10 pp 163 - 168, **1992**

Binning, G.; Quate, C. F.; Gerber, C., Phys. *Rev. Lett.*, **1986**, 56, p930

Burrows, V.A.; Chabal, Y.J.; Higashi, G.S.; Raghavachari, K. and Christman, S.B. *Applied Physics. Letter.* **1988**, 53, 998.

Chabal, Y.J.; Higashi, G.S.; Raghavachari, K. and Christman S.B. *Journal of Vacuum Science and Technology*, **1989**, A7, 2104.

Christy, A.G.; Lowe, A.; Otieno, V.; Otieno-Alego, V.; Stoll, M. and Webster, R.D. *Journal of Applied Electrochemistry* 34: 225-233, **2004**

Chyan, O.; Chen, J. and Chien, H *J Electrochem. Soc.*, **1996,**143, 1.

CiCileo, G. P.; Grepo, M.A.; Rosales, B.M. *Corrosion Science* 46 (**2004**), 929-953.

"Copper." Wikipedia: http://en.wikipedia.org/wiki/Copper. Retrieved on March, **2009**.

Cotton, F.A.; Murillo, C.; *Advanced Inorganic Chemistry*, John Wiley & Sons; New York, **1999**.

"Cyclic voltammetry." Wikipedia: http://en.wikipedia.org/wiki/Cyclic_voltammetry. Retrieved on March, **2009**.

Delgado, J. M.; Orts, J. M.; Rodes, A. *Langmuir* **2005**, 21, 8809.

Edwards, H.W. and Petersen, R.P. *Phys. Rev.* 50 (9) 871, **1936**

Electroless plating". Wikipedia: http://en.wikipedia.org/wiki/Electroless_plating. Retrieved on March, **2009.**

Farshad, F. F.; Pesacreta, T. C. *Anti-Corrosion Methods and Materials.* **2003** 50: 6-60

Fitzgerald, K. P.; Nairn, J. and Atrens, A. *Corrosion Science*, Vol. 40, No. 12, pp. 2029-2050, **1998**

Frommer, J.; Meywer, E. *J. Phys.*: Condens. Matter, 3, S1-S9 **1991**.

FT-IR Spectroscopy—Attenuated Total Reflection (ATR). *Perkin Elmer Life and Analytical Sciences*, **2005**.

Génin, J.; Ruby, C.; Géhin, A.; Refait, P. *C. R. Geoscience.* 338 (**2006**) 433–446

Harrick, N.J., *Internal Reflection Spectroscopy*, Interscience Publishers, NY, **1967**.

Hartinger, S. and Doblhofer, K. *Journal of Electoanalytical Chamistry*, 380(**1995**) 185-191

Hatta, A.; Sasaki, Y.; Suetaka, W. *J. Electroanal. Chem.* **1986**, *215*, 93.

Hertwig, R. H.; Koch, W.; 1der, D. S.; Schwarz, H. *J. Phys. Chem.*, Vol. 100, No. 30, **1996**

Hong, X; *Introduction to Semiconductor Manufacturing Technology,* Prentice-Hall Inc., Upper Saddle River, New Jersey, **2001.**

Huang, L.; Bohannan, E.; Huang, C. and Switzer, J. *Israel Journal of Chemistry* Vol. 37 **1997** p293-301

Huo, S.; Xue, X.; Li, Q.; Xu, S. and Cai, W. *J. Phys. Chem. B,* Vol. 110, No. 51, **2006.**

Juodkazyte, J.; Vilkauskaite, R.; Stalnionis, G.; Sebeka, B.; Juodkazis, K. *Electroanalysis* 19, **2007**, No. 10, 1093 – 1099

Kalvoda, R. and Parsons R., *Electrochemistry in Research and Development*, New York: Plenum press, **1985**.

Kershen, K.; Celio, H.; Lee, I.; White, J. M. *Langmuir*, **2001**, 17, 323-328.

King, F.; Quinn, M.J.; Like, C.D. *Journal of Electroanalytical Chemistry* 385(**1995**) 45-55

Kirkpatrick, J. *Burns,* vol. 21, No. 7 pp 483 - 493, **1995**

Lee, C.; Qina, Z.; Odziemkowski, M.; Shoesmith, D. *Electrochimica Acta* 51 (**2006**) 1558–1568

Lee, I.; Bae, S.; Song, M.; Lee, I.; Paek, S.; and Lee, C. *Bull. Korean Chem. Soc.* **2004**, 25, 2.

Lee, J. and Tak, Y. *Electrchemical and Solid- State Letter*. 2(11) 559-560 (**1999**)

Malvault, J. Y and Lopitaux, J. *Jounal of Applied Electrochemistry* 25(**1995**) 841-845

Martin, Y.; Wichramasinghe, H. K. *Appl. Phys. Lett*. **1987**, 50, 1455

Meyer, F. and White, J. *Semiconductor International*, Silicon Engineering Technology Center Laboratory, **1999**, July, 137.

Mirabella, F.M.; Harrick, N.J. *Internal Reflection Spectroscopy; Review and Supplement*, Harrick Scientific Corporation, N.Y. **1985**.

Nikolic, J.; Expósito, E.; Iniesta, J.; González-García, J. and Montiel, V. *Journal of Chemical Education*. Vol. 77 No. 9 September **2000**

Noil, F.; Misaelides, P.; Hatzdimitriou, A.; Pavlidou E. and Kokkorris, M. *J. Mater. Chem*. **2003**, 13, 114-120

Noli, F.; Misaelides, P.; Hatzidimitriou, A.; Pavlidou, E. and Kokkoris, *M. J. Mater. Chem.,* **2003**, 13, 114-120

Orozco, G.; Perez, M. C.; Rincon, A.; Gutierrez C. *Langmuir*, **1998**, 14, 6297-6306.

"Patina" Merriam-Webster on-line dictionary; http://www.merriam-webster.com/ Updated by March, **2009**

"Patina." Wikipedia: http://en.wikipedia.org/wiki/Patina. Retrieved on March, **2009.**

Petrucci, R. H. *General Chemistry: Principles & Modern Applications* (9th edition). Prentice Hall. pp. 606. **2007**.

Peulon, S. and Lincot, D. *J. Electrochem. Soc.,* Vol. 145, No. 3, March **1998**

"Piranha solution." Wikipedia: http://en.wikipedia.org/wiki/Piranha_solution. Retrieved on March, **2009**.

"Plating." Wikipedia: http://en.wikipedia.org/wiki/Plating. Retrieved on March, **2009.**

"Platinum." Wikipedia: http://en.wikipedia.org/wiki/Platinum. Retrieved on March, **2009**.

Pool, R. *Science*, **1990**, 247, 634.

"Pourbaix diagram." Wikipedia: http://en.wikipedia.org/wiki/Pourbaix_diagram. Retrieved on March, **2009.**

Rodes, A.; Orts, J. M.; Perez, J. M.; Feliu, J. M.; Aldaz, A. *Elctrochem. Commun.* **2003**, 5, 56.

Rojluechai, S.; Chavadej, S.; Schwank, J. W.; Meeyoo, V. *Catalysis Communications.* 8 (**2007)** 57–64

"Rotating disk electrode." Wikipedia: http://en.wikipedia.org/wiki/Rotating_disk_electrode. Retrieved on March, **2009**.

"Roughness." Wikipedia: http://en.wikipedia.org/wiki/Roughness Retrieved on March, **2009.**

Runyan, W.R.; Bean K.E; *Semiconductor Integrated Circuit Processing Technology*; Addison-Wesley Publishing Company: Reading, **1990**.

"Ruthenium." Wikipedia: http://en.wikipedia.org/wiki/Ruthenium. Retrieved on March, **2009**.

Schlesinger, R.; Klewe-Nebenius H. and Bruns, M. *Surface and Interface Analysis* 30, 135-139 (**2000**)

"Silicon." Wikipedia: http://en.wikipedia.org/wiki/Silicon. Retrieved on March, **2009**.

"Silver." Wikipedia: http://en.wikipedia.org/wiki/Silver. Retrieved on March, **2009**.

Simon, L.; Genin, J. and Refait, P. *Corrosion Science*, Vol. 39, No. 9, pp. 1673-1685, **1997**

Sugawara, Y.; Yadav, A.; Nishikata, A. and Tsuru, T. *Journal of Electrochemical Society*, 155 (9) B897-B902 (**2008**)

Switzer, J.; Huang, C.; Huang, L.; Miller, F.; Zhou, Y.; Raub, E.; Shumsky M.; and Bohannan, E. *J. Mater. Res*, Vol. 13(4) 911-916(**1998**)

"The periodic table." webelements.com: http://www.webelements.com/. Retrieved on Feburary, **2008**.

Veleva, L.; Quintana, P.; Ramanaluskas, R.; Pomes R. *Electrimica, Acta*, 41(10) 1641-1646 (**1996**)

"Voltammetry." Wikipedia: http://en.wikipedia.org/wiki/Voltammetry#Three_electrode_system. Retrieved on March, **2009**.

Vukmirovic, M. B.; Dimitrov, N.; Sieradzki, K., *J. Electrochem. Soc*, **2003**. 150 (1): p. B10-B15.

Weaver, M. J.; Barz, F.; Gordon, J. G., II; Philpott, M. R. *Surf. Sci.* **1983**, *125*, 409.

Wickramashinghe, H. K. *Sci. Am.*, **1989**, 98.

Woods, I. *The Elements: Platinum*. Benchmark Books. **2004**

Ye, S.; Ichihara, T. and Uosaki, K. *Journal of the Electrochemical Society*, **2001,**148**,** 6, C421-C426.

Zavala, G. *Colloid Polym Sci*. **2008** 286:85–95

Zhang, Y.; Ojeda, O.; Flores, S.; Arunagiri, T.; Chyan, O. "Study of Cu Complex Formation on the Ruthenium Surface using Cyclic Voltammetry and X-ray Photoelectron Spectroscopy" Abstracts, 60th Southwest Regional Meeting of the American Chemical Society, Fort Worth, TX, United States, September 29-October 4 (**2004**)

Zhang, Y.; Venkataraman, S.; Chyan, O. “Investigation of electrochemical copper patination on noble metal surfaces” Abstracts of Papers, 231st ACS National Meeting, Atlanta, GA, United States, March 26-30, **2006**